E&G Quaternary Sci. J., 74, 235–262, 2025 https://doi.org/10.5194/egqsj-74-235-2025 © Author(s) 2025. This work is distributed under the Creative Commons Attribution 4.0 License.





# Silts with a human touch: the shift from natural to anthropogenically controlled fluvial dynamics in the Kinzig River floodplains, southwestern Germany

Charlotte E. Engelmann<sup>1</sup>, Frank Preusser<sup>2</sup>, Alexander Fülling<sup>2</sup>, Jakob Wilk<sup>2</sup>, Elisabeth Eiche<sup>3</sup>, Dennis Quandt<sup>3,a</sup>, Stefan Hergarten<sup>2</sup>, and Jan H. Blöthe<sup>1</sup>

**Correspondence:** Charlotte E. Engelmann (charlotte.engelmann@geographie.uni-freiburg.de)

Received: 26 February 2025 – Revised: 15 September 2025 – Accepted: 21 September 2025 –

Published: 12 November 2025

How to cite: Engelmann, C. E., Preusser, F., Fülling, A., Wilk, J., Eiche, E., Quandt, D., Hergarten, S., and Blöthe,

J. H.: Silts with a human touch: the shift from natural to anthropogenically controlled fluvial dynamics in the Kinzig River floodplains, southwestern Germany, E&G Quaternary Sci. J., 74, 235–262,

https://doi.org/10.5194/egqsj-74-235-2025, 2025.

**Abstract:** 

Central European fluvial systems shifted from naturally to anthropogenically controlled during the middle to late Holocene, responding uniquely to non-synchronous and interdependent natural and anthropogenic forcings. Previous research mainly focused on either large river systems or small catchments, yet meso-scale systems linking these have received little attention so far. Floodplains constitute an ideal setting to address this issue as their sediments recorded past river dynamics and human activity. This study investigates the transition from natural to anthropogenic control in the meso-scale Kinzig River in southwestern Germany using a combination of sedimentology, geochemical analysis, luminescence dating, and geophysical surveys. In the Kinzig catchment, three phases of floodplain accumulation are identified with characteristic sedimentation rates: late Pleistocene-early Holocene until 9.0 ka (0.1 mm a<sup>-1</sup>), middle-late Holocene from 9.0 until 0.82 ka (0.3 mm a<sup>-1</sup>), and the modern era from 0.82 ka until current times (1.1 mm a<sup>-1</sup>). Characterising these phases are decreasing grain sizes and increasing heavy metal concentrations (barium, lead, copper) in overbank fines, correlating with historical mining activity (peaking in the 16th and 18th centuries). This indicates the impact of mining on sediment delivery via deforestation that caused hillslope instability and sediment contamination. A cross-reference of floodplain stratigraphy with the catchment land use history reveals a gradual shift to an anthropogenically altered system, with intensified human impacts over the last 1000 years, approximately. This aligns with high floodplain sedimentation rates related to human presence. These findings depict the timing and dynamics of anthropogenic impacts on meso-scale fluvial systems in previously natural landscapes.

<sup>&</sup>lt;sup>1</sup>Institute of Environmental Social Sciences and Geography, University Freiburg, Freiburg, Germany

<sup>&</sup>lt;sup>2</sup>Institute of Earth and Environmental Sciences, University of Freiburg, Freiburg, Germany

<sup>&</sup>lt;sup>3</sup>Institute of Applied Geosciences, Karlsruhe Institute of Technology, Karlsruhe, Germany

<sup>&</sup>lt;sup>a</sup>now at: Geschäftsstelle Länderarbeitskreis Energiebilanzen, Statistisches Landesamt Baden-Württemberg, Fellbach, Germany

#### **Kurzfassung:**

Mitteleuropäische Flusssysteme wandelten sich während des mittleren bis späten Holozäns von natürlich zu anthropogen kontrollierten Systemen, wobei sie einzigartig auf nicht-synchrone und voneinander abhängige natürliche und anthropogene Einflüsse reagierten. Bisherige Forschungen konzentrierten sich hauptsächlich entweder auf große Flusssysteme oder kleine Einzugsgebiete, während mesoskalige Systeme, die diese verbinden, bislang wenig Beachtung fanden. Auen stellen ein ideales Umfald dar, um diese Fragestellung zu untersuchen, da ihre Sedimente frühere Flussdynamiken und menschliche Aktivitäten aufzeichnen. Diese Studie untersucht den Übergang von natürlich zu anthropogen gesteuerten Systemen im mesoskaligen Kinzig-Fluss in Südwestdeutschland unter Verwendung einer Kombination aus Sedimentologie, geochemischer Analyse, Lumineszenzdatierung und geophysikalischen Untersuchungen. Im Kinzig-Einzugsgebiet wurden drei Phasen der Auenakkumulation mit charakteristischen Sedimentationsraten identifiziert: Spätes Pleistozän/Frühes Holozän bis  $9.0 \,\mathrm{ka} \, (0.1 \,\mathrm{mm} \,\mathrm{a}^{-1})$ , Mittel-/Spätholozän von  $9.0 \,\mathrm{ka}$  bis  $0.82 \,\mathrm{ka} \, (0.3 \,\mathrm{mm} \,\mathrm{a}^{-1})$  und Modern von 0,82 ka bis zur Gegenwart (1,1 mm a<sup>-1</sup>). Passend zu diesen Phasen sind abnehmende Korngrößen und zunehmende Schwermetallkonzentrationen (Barium, Blei, Kupfer) in den Überflutungssedimenten, deren mit der historischen Bergbautätigkeit korrelieren (Höhepunkte im 16. und 18. Jahrhundert). Dies deutet auf den Einfluss des Bergbaus auf die Sedimentzufuhr durch Entwaldung hin, der Hanginstabilität und Sedimentkontaminationen verursachte. Ein Abgleich der Auenstratigraphie mit der Landnutzungsgeschichte des Einzugsgebiets zeigt eine allmähliche Verschiebung zu einem anthropogen veränderten System mit intensiviertem menschlichem Einfluss in den letzten ca. 1000 Jahren. Dies stimmt mit hohen Ablagerungsraten in der Aue überein, die mit der menschlichen Präsenz zusammenhängen. Diese Ergebnisse verdeutlichen den zeitlichen Verlauf und die Dynamik anthropogener Einflüsse auf mesoskalige Flusssysteme in ehemals natürlichen Landschaften.

#### 1 Introduction

Fluvial systems in central Europe changed from a naturally to anthropogenically controlled regime predominantly during the middle to late Holocene. As floodplain sediments recorded past river dynamics and human activity (e.g. Brown et al., 2013), studying their stratigraphy has shown that, in Europe, these were transformed over a long time period by diverse drivers during varying phases (Brown et al., 2018). High pressure on the functioning of fluvial environments is indicated by the loss of ca. 95% of European floodplain ecosystems due to intensive land use and river training (Tockner et al., 2022). A large body of research of the past decades documents direct (e.g. dams, straightening, embankments) and indirect (e.g. agriculture, deforestation, mining) anthropogenic impacts on fluvial systems (e.g. Kalis et al., 2003; Zolitschka et al., 2003; Starkel et al., 2006; De Moor et al., 2008; Walter and Merritts, 2008; Dotterweich, 2008; Macklin et al., 2010; Notebaert and Verstraeten, 2011; Brown et al., 2013, 2018; Gibling, 2018; Maaß et al., 2021; Hohensinner et al., 2022; Elznicová et al., 2023). Floodplain transformation in response to natural (climatic shifts) and anthropogenic forcings, however, was neither uniform nor synchronous. Specifically, river catchments show nonsynchronous and interdependent adaption that does not have a concurrent European-wide or even catchment-wide onset under similar triggers (Brown et al., 2018; Fuchs et al., 2010; Stolz et al., 2013; Broothaerts et al., 2014; Hoevers et al., 2024). Previous research investigating human impacts on soil erosion and floodplain deposition mainly focused either on large (>  $10^4$  km²) river systems (e.g. Houben et al., 2006; Starkel et al., 2006; Hoffmann et al., 2007b; Holzhauer et al., 2017) or on small-scale (<  $10^2$  km²) catchments (Fuchs et al., 2011; Houben, 2012; Larsen et al., 2013). However, how and when meso-scale catchments ( $10^2$ – $10^4$  km²) transitioned from naturally to anthropogenically controlled fluvial systems remains poorly investigated.

The Rhine River is one of the largest drainage systems of Europe (Fig. 1A), with its sediments having recorded tectonic developments, climatic changes, and anthropogenic activities (Preusser, 2008). The modern floodplains developed after the Pleistocene-Holocene transition, and sedimentation rates increased with anthropogenic settlement due to stronger erosion in the catchments starting ca. 7500 years ago (e.g. Hoffmann et al., 2007b; Lang et al., 2003). Agricultural areas in the Upper Rhine area extended notably during the Bronze Age (2200–800 BCE) and the Iron Age (800– 15 BCE), whereas the Celts cleared woodland for the first time on large scales and mined ores during the period of the La Tène (450–0 BCE) culture (e.g. Hoffmann et al., 2007b; Lang et al., 2003; Mäckel et al., 2009). In particular, agricultural extension and deforestation increased soil erosion during the pre-Roman Iron Age and Roman period (1–350 CE) as the bare land surface was subsequently more susceptible to soil erosion (e.g. Hoffmann et al., 2007b; Lang et al., 2003). Consequently, higher sediment input into fluvial systems affected sediment budgets and led to increasing sedimentation rates on floodplains (e.g. Dotterweich, 2008; Macklin et al., 2010; Stolz et al., 2013; Notebaert et al., 2018). The characteristic flood loams (clayey, silty, and sandy sediments) are considered to be the result of Holocene hillslope erosion that shows a lithological difference compared to the underlying Pleistocene sand and gravel (Hoffmann et al., 2007a).

On a regional level, the richness of valuable ores in the Black Forest and Vosges Mountains bordering the Upper Rhine area (Fig. 1B and C) resulted in extensive mining and processing that caused the emission of metal and metalloid compounds via smelting, accumulation of waste material, and dewatering of mines (e.g. Markl, 2016; LUBW, 2014). Metal and metalloid compounds either get attached to sediments and stored in reservoirs (e.g. floodplains, lakes) or are gradually and repeatedly distributed over long distances by fluvial systems (up to 100 km downstream from miningdischarge sites; Macklin et al., 2023) long after mining has ceased (e.g. Wohl, 2015). Additionally, direct channel and floodplain modifications were initiated to improve drainage and navigability during the early post-Roman period. In the Black Forest, the timber drift and rafting economy played an important role in impacting channel erosion, discharge, sediment connectivity, and channel roughness (e.g. Wohl, 2015; Steinle and Herbener, 2016; Belletti et al., 2020; Galia, 2021; Maaß et al., 2021; Werther et al., 2021).

The majority of previous studies in the Upper Rhine area have focused on fluvial dynamics and human land use in the main plain (e.g. Lang et al., 2003; Hoffmann et al., 2007a, 2009; Euzen et al., 2024; Abdulkarim et al., 2024) rather than on its tributaries. Hence, it remains largely unknown when the Upper Rhine tributaries were affected by human impact, whether this correlates with high floodplain sedimentation rates, and if contaminations from mining in floodplain sediments reflect the pathways of human impact on the fluvial system. Here, we use a combination of sedimentological investigations, geochemical analysis, luminescence dating, and geophysical surveys to investigate the geomorphological history of a meso-scale Rhenian catchment, focusing specifically on the shift from a natural to an anthropogenically controlled fluvial system. The Kinzig River has experienced extensive and historic anthropogenic land use pressure (forestry, mining) that allows us to address the onset of the deposition of anthropogenically conditioned sediments (James, 2013; Macklin et al., 1994). Floodplain stratigraphy was gathered and interpreted in the context of regional- and catchment-scale historic documents on land use practices. Ultimately, the aims of this study are to achieve an understanding of the natural fluvial system and to discuss the transition under human impacts. Specific focus is placed on the search for the onset of the deposition of anthropogenically conditioned sediments and the local conditions of floodplain contamination by heavy metals.

# 2 Regional setting

# 2.1 Kinzig catchment

The Kinzig River is the largest (ca. 1400 km<sup>2</sup>) fluvial system draining the mid-mountain range of the Black Forest in southwestern Germany (Fig. 1B). Descending from the heights of the Black Forest in the east to the confluence with the Rhine River near the city of Kehl in the west (Fig. 1B), the catchment covers an altitudinal range from 1081 to 156 m above sea level (ma.s.l.). The pluvio-nival character of the Kinzig River gives a generally high discharge in winter and low discharge in summer (LUBW, 2024), with many historical floods being the result of lasting phases of heavy precipitation and snowmelt (Bösmeier at al., 2022). The upstream sections of the Kinzig River (most tributaries and the area upstream of the village of Schenkenzell) are characterised by steep slope gradients that confine the channel beds and floodplain widths (occasionally < 100 m), contrasting to the wider (ca. 1500 m) downstream sections (downstream of the town of Wolfach; Fig. 1B).

## 2.2 Geological setting

The Kinzig River system (Fig. 1B and C) is located at the eastern shoulder of the Upper Rhine Graben (URG), an SSW-NNE-oriented rift valley extending over 300 km within the central part of the European Cenozoic Rift System (Ziegler, 1994). It is bound between the Jura Mountains in the south, the Rhenish Massif in the north, and the graben shoulders in the east (Black Forest) and in the west (Vosges; Fig. 1B) (Preusser, 2008). The Alpine Orogeny initiated crustal thinning in the Upper Rhine Plain and the graben development during the Late Mesozoic. Simultaneous subsidence of the graben and uplift of the shoulders started in the Eocene. Whereas the graben is filled with Tertiary and Quaternary sediments, the shoulders have a Variscan crystalline basement, mainly gneiss and granite, covered by siliciclastic rocks of the Buntsandstein (Triassic red sandstone). The Rhine River flowing in the graben plain shifted between braided and anastomosing or meandering patterns during cold and warm periods of the Quaternary (Dambeck and Thiemeyer, 2002).

Three NE–SW-oriented zones roughly subdivide the catchment geology of the study area (Fig. S1 in the Supplement). The stream network cuts through Palaeozoic magmatites and middle to upper Buntsandstein in the eastern zone. The middle zone comprises Palaeozoic gneisses and magmatites. Lower and middle Buntsandstein rocks with some Permian sediments (mainly sandstones) characterise the western zone, with some local occurrences of leucocratic gneiss and paragneiss (LGRB, 2024). Common ores in the catchment are lead–zinc–copper–fluorite–barite and lead–barite–quartz–fluorite (e.g. Markl, 2016).

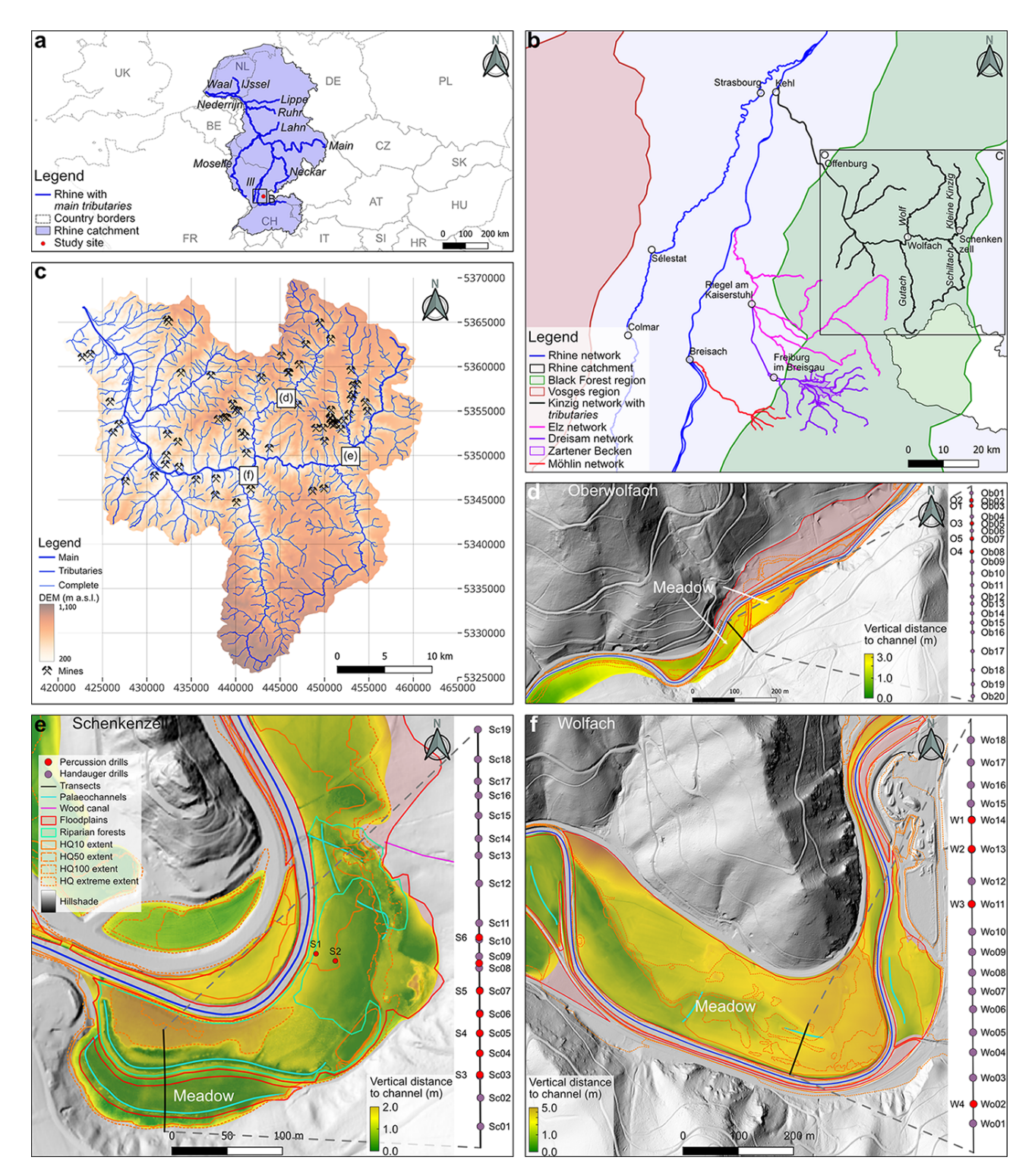


**Figure 1.** Geographical setting of the study area. (a) Rhine catchment, including main tributaries and study area (rectangle). (b) Study region within the Black Forest, including tributaries and settlements. (c) Kinzig catchment, with stream network, elevation, field sites, and historical mining locations (sources: Fig. S10 in the Supplement). (d–f) Study sites with floodplain areas, including vertical distance to the current channel (m), transects with drill positions, location of palaeochannels, outline of riparian forests, HQ (flood) event extents, and location of wood canal. Transect lengths: 85 m (Schenkenzell), 78 m (Oberwolfach), and 142 m (Wolfach). The vertical distance along transects is given in Fig. 9. The coordinates of the field sites (e.g. drills, transects) are given in Table S1 in the Supplement. A geological map of the catchment is given in Fig. S1. The localisation of mined material is provided in Fig. S10 and Table S8.

## 2.3 Anthropogenic impact and floodplain use

Early human impact in the Rhine River system started about 7500 years ago (e.g. Hoffmann et al., 2007b; Lang et al., 2003) and might have been simultaneous in the Kinzig catchment. One important reason for humans to modify the Kinzig stream network directly was the need to lower the threat of recurring floods (Bösmeier et al., 2022). The river underwent radical modifications in the river rectification programme, led by the engineer Johann Gottfried Tulla in the early 19th century, for discharge observation, flood protection, and expansion of arable area (e.g. Himmelsbach, 2012; Stalf, 1932). These modifications had a strong land use impact, particularly on timber drift and raft. The companies orchestrating that economy ("Flößerei-Genossenschaften") directly stimulated catchment deforestation. Mainly in winter, oak and spruce trees were cut and transported to streams via cards or wood slides ("Riesen"). In spring, the timber was floated downstream by controlling the discharge using a network of weirs and sluices. This happened in hand with modifying and clearing the riverbanks and channel beds and the installation of channel barriers (e.g. Konold et al., 2019; Barth, 1895; Lehmann, 2005; Harter, 2011; Schauenburg, 1899; Scheifele, 1995a).

Widespread deforestation of floodplains and hillslopes was carried out for gathering natural resources and construction by large landowners and locals. Such anthropogenic impacts resulted in regionally increased alluvial sedimentation during the 10th–12th century when medieval monastic and manorial colonisation prevailed (Mäckel et al., 2009). Widespread deforestation in the Kinzig catchment occurred from at least the 16th century, and European timber trade intensified in the late 17th century, decimating oak populations at high Black Forest elevations alongside widespread local overlogging in the middle and southern Black Forest (Konold et al., 2019; Longoni, 2024).

Simultaneously, historic mining, metallurgic processes, and charcoal production occurred mainly upstream along the Kinzig (Ludemann, 2010). The earliest regional mining structures date back to ca. 200 BCE-190 CE (Markl, 2016). Mining of mainly silver (Ag) intensified during the 11th century and peaked during the 13th and 16th centuries (Markl, 2016), during which time mines were also reopened, adding further pressure to the forests due to the use of timber for construction and ore processing (e.g. Werner and Dennert, 2004; Markl, 2016; Straßburger, 2017; Knausenberger, 2001). Additionally, timber was highly demanded for the construction of buildings, fuel, and charcoal production, including for markets abroad (e.g. Schauenburg, 1899; Barth, 1895; Scheifele, 1995b; Steinle and Herbener, 2016; Longoni, 2024). Therefore, historical mining in the Kinzig catchment directly drove deforestation and, thus, likely enhanced fine sediment transport to the stream network and floodplains and introduced metal-contaminated flood loams.

## 2.4 Study sites

The study focuses on three floodplains (Fig. 1D–F) within the Kinzig catchment, of which two are located along the main channel, and one is located along the Wolf tributary (Fig. 1B). The selection of upper and middle channel reaches reduces the complexity of accumulating and interfering with sedimentological signals from the multitude of tributaries near the Rhine confluence. The specific floodplains were chosen based on the relatively short sediment transport distances from anthropogenic land use hotspots, namely downstream positions from (mainly historic) mines, channel barriers (e.g. weirs, sluices), and historic timber drift and raft sites.

The Wolfach site is the most downstream location, 2.9 km downstream of the Wolf and Kinzig confluence and 1.3 km upstream of the confluence with the Gutach tributary (Fig. 1B) and F). Both the valley and floodplain are relatively wide (ca. 290 m), and the studied area is located at the inner river bend. Around half of the total floodplain width (ca. 150 m) was studied, specifically the section closest to the channel that accommodates full flooding during HQ100 events (flood occurrence once in 100 years; LUBW, 2024). The whole floodplain width (ca. 290 m, including the northern area after a 1 m elevation step) floods during HQ extreme events (rarer than HQ100; LUBW, 2024). The upstream city of Wolfach was vital for the timber drift and rafting companies, organising the trade with, among others, the city of Strasbourg and, further downstream, the Rhine to the Netherlands (Scheifele, 1995a).

The Schenkenzell site is the most upstream location along the main Kinzig valley, with a summed floodplain width from both sides of the river of ca. 150 m (Fig. 1E). Here, the wider and less constructed southern floodplain along the outer meander bend was regarded to be the most suitable to study. The light detection and ranging (lidar) data reveal palaeochannels in the riparian forest, located between the meadow and channel that is partly covered by the transect (Fig. 1E). A historic map from the year 1816 CE (Fig. S11) shows a weir (remnants still present) in this river bend that diverts the streamflow along the southern floodplain edge. On another map from the year 1896 CE (Figs. S12 and S13), this stream had a weir and was named "Schenkenzeller Holzkanal" (wood canal), indicating its importance as a timber raft binding site. The timber was transported here via a wood slide that ended just southeast of the floodplain, close to the divergence of the Kinzig and wood canal (Fig. 1E), and weirs controlled the discharge for timber transport. Several large mines upstream of Schenkenzell are potential sources for contaminated sediments (Figs. 1C and S10, Table S8). While the present-day floodplain accommodates flooding of extremity HQ50 (flood occurrence once in 50 years; LUBW, 2024) or higher, HQ extreme events also flood the riparian forest.

The Oberwolfach site is located along the Wolf tributary and has a confined floodplain with a maximum width of ca.

90 m inside a narrowly incised valley (Fig. 1D). Studying this floodplain relative to the Schenkenzell site allows us to analyse the impact of different degrees of mining intensity on the floodplain stratigraphy. Here, the upstream area was less extensively mined than in Schenkenzell (Figs. 1C and S10, Table S8). Additionally, the transect incorporates the hillslope to better grasp the thicknesses of colluvial deposits that potentially contribute to the floodplain fine thickness. The current floodplain elevation accommodates flooding of at least the lowest half of the floodplain during HQ10 (flood occurrence once in 10 years; LUBW, 2024) events. Deposition of boulders with diameters (*d*) up to 1 m occurred during a flood in the years of 1991–1992 CE (personal communication with local farmer, 31 May 2024).

# 3 Methodology

#### 3.1 Sediment sampling

Floodplain sediment variability was studied along a transect perpendicular to the channel with a minimum of four percussion drillings and additional hand augering (Fig. 1D–F). Sediment cores were recovered in opaque plastic liners (outer  $d=6\,\mathrm{cm}$ , inner  $d=5.4\,\mathrm{cm}$ ) that were closed off in the field to allow for luminescence dating. Aside a rough average spacing of hand augerings between percussion drillings, additional spots were investigated at features of interest, as shown in the geophysical measurements (e.g. palaeochannels, dipping or rising structures). All percussion drillings were made using an electric-powered percussion hammer (Milwaukee K 2500 H) until a maximum penetration depth was reached due to the presence of cobbles or gravel bodies. A differential TRIMBLE R12 (DGNSS) was used to georeference the drilling sites and to determine the transect lengths.

The sediment cores were studied in the laboratory after cutting the liners under red-light conditions. One half was sampled for luminescence, and the other half was sampled for sedimentological and geochemical analyses. Further details on the sample handling are provided in Sect. S2.1 in the Supplement. In total, 297 samples were taken for infrared stimulated luminescence (IRSL) screening, and 13 were taken for optically stimulated luminescence (OSL) dating. The cores were photographed using the setup of Gegg and Gegg (2023) and were systematically logged (e.g. Munsell dry colour and rough grain size classification) before geochemical screening and sampling for sedimentological and geochemical analyses. The amount of available sample material defined whether all analyses could be applied, prioritising the geochemical measurements. In total, 340 sedimentological samples were taken, of which 79 were used for energy-dispersive X-ray (EDX) spectroscopy measurements. The correction of compaction in the liners entails core-specific linear compaction intervals (per core metre) based on the discrepancy between the drilled depth in the field and the core material depth in the liner.

# 3.2 Grain size and organic matter content

Grain size was measured with a Malvern Mastersizer 3000 laser particle size analyser with a wet dispersion unit (particle size range: 0.01-3500 µm). Sample preparation included drying at 60 °C for several days, dry sieving to < 1 mm to avoid clogging, and removal of organics using 15 % H<sub>2</sub>O<sub>2</sub>. Carbonate was not destroyed as testing the material with HCl indicated very little to no carbonate. Samples were diluted with distilled water before being completely dried at 60 °C. Subsequently, the addition of 50 mL of Calgon per sample dispersed the materials before setting them for 24h until recording the Mastersizers' background signal of just the circulating water (Abdulkarim et al., 2021). Material was added slowly into the units' tap water until reaching the desired obscuration range. Three measurements were carried out per sample, except for remeasuring outliers. The results were finally analysed in the GRADISTAT v. 8.0 program (Blott and Pye, 2001).

Organic matter (OM) and carbonate contents were determined with the loss on ignition (LOI) method, following Heiri et al. (2001), aside from removing large organic fragments during sieving; ca. 1 g of fine-grained material and 3 g of coarse-grained material were used, respectively. The larger sample size for coarse material was used to achieve a better OM content representativeness. Overestimation of OM contents by structural water loss is expected to be negligible due to the low clay content (catchment geology; Fig. S1), especially in the upper soil horizons that are likely to be rich in OM and heavy elements (Heiri et al., 2001; Sun et al., 2009).

## 3.3 Geochemical analyses

Concentrations of elements in the cores were measured in situ using a Bruker S1Titan800 portable X-ray fluorescence (pXRF) analyser after air-drying the cores at room temperature for 14 d. In general, the approach described in Quandt et al. (2024) was followed and adjusted to the specifics of the sample material. The measurements at 5 cm intervals along the cores allowed us to identify promising samples for the EDX spectroscopy analyses. In contrast to the high density yet relative pXRF data, the lower-density yet absolute EDX data are suitable for quantitative comparison. Further details on the measurement procedure are provided in Sect. S4.1. In total, 294 pXRF measurements were made of the sediment matrix, aside from 12 component measurements (e.g. cobbles, metal objects).

Subsampling for sedimentological and geochemical analyses at, generally, 5 cm intervals considered the stratigraphic layers. The results of pXRF and IRSL screening (Sect. 4.1) assisted in the identification of depths of interest to collect ca. 7 g material for the geochemical EDX spectroscopy measurements. These depths of interest are mainly where the heavy metal concentration trends change in modern (recently deposited) sediments, as predetermined with pXRF, aside from samples to establish the prehuman-impact background con-

centrations. Measurements were done at the KIT Laboratory for Environmental and Raw Materials Analysis (LERA), Karlsruhe, Germany. Further details on sample preparation and measurement procedure are provided in Sect. S4.2.

The EDX and pXRF data formed the basis to compute element–depth trends in the cores. Comparisons of these datasets were based on statistical tests and parameters in RStudio (version 4.5.1). Firstly, as a trend description, linear and logarithmic concentration–depth models were fitted on element or core categories, of which the fit was quantified with the coefficient of determination ( $R^2$ ). Secondly, the Pearson (r) and Spearman's rank correlation coefficients were computed for quantification and direction of the datasets' association in cores with at least three EDX data points for the primarily studied elements (Ba, Pb, Cu; Table S6). The data processing steps are provided in Sect. S4.3. Note that, here, barium is referred to as heavy metal for ease of readability, although it is, strictly speaking, a heavy alkaline Earth metal.

Referring to elevated heavy metal concentrations in sediments is only possible relative to reference or background values. These are often regionally determined thresholds (e.g. Bodenschutz, 2017) in relation to natural geogenic input. However, such threshold values do not take into account small-scale variability from factors such as local geology and local atmospheric and fluvial deposition. One way to tackle this challenge is by computing enrichment factors (EFs) for individual cores that use a reference element when studying elevated concentrations. Although these are flawed themselves (Reimann and de Caritat, 2005), they do account for grain size and mineral composition influences by double normalisation when only considering same-core background values (e.g. Grygar et al., 2013; Weber and Lehmkuhl, 2024). Minimum anthropogenic impact or natural background values are indicated with EF = 1.0. Here, heavy metal concentrations of overbank fines from the deepest samples (Pleistocene to early Holocene) were used as background values, of which the most suitable reference element was vanadium (V; Table S4). Further details on the determination of the reference element are provided in Sect. S4.4.

Finally, studying linear correlations by performing a principal component analysis (PCA) supported the investigation of whether the heavy element trends are predictable by other material characteristics. Correlations between the individual and combined variables were analysed as the PCA represented the data in smaller sets of variables while maintaining the strongest variations among samples. Further details on the computation, outcomes, and discussion are provided in Sect. S4.5.

# 3.4 Geochronology

A range of dating techniques was applied to the floodplain sediments. IRSL screening gives a rough age estimate (relative to the year 2024) when measuring the natural IRSL signal  $(L_n)$  and normalising it by a known test dose  $(T_n)$ . The  $L_{\rm n}/T_{\rm n}$  ratio allows us to estimate the absorbed irradiation dose as long as signal growth is close to linear, the dose rate is approximately known, and the effect of fading is neglected (May et al., 2015). The method has proven to be useful for identifying changes in sedimentation rates, hiatuses, and indications of partial bleaching in sediment records from the Upper Rhine region (Schulze et al., 2022; Schwahn et al., 2023; Abdulkarim et al., 2024). Sample collection for IRSL screening at 5 cm intervals occurred after scraping away the surface exposed to sunlight and then drying at 50 °C for 24 h and gently homogenising using a mortar and pestle. Three aliquots per sample were measured on steel discs stamped with silicon oil (d = 6 mm). Finally, measurements were performed with one cycle of the single-aliquot regenerative dose (SAR) procedure by Murray and Wintle (2003) on a Risø reader, using a preheat of 250 °C for 60 s, IR stimulation at 50 °C for 70 s, and a test dose of ca. 20 Gy.

Consecutively, the  $L_n/T_n$  ratios were used to determine the best samples for OSL dating in three "main" cores (W1, W2, S5) that were chosen based on the core location in the floodplains and maximum depths. These cores were sampled with cleaned surfaces over 6 cm lengths, accounting for a minimum of 70 g dried material for determination of the equivalent dose  $(D_e)$ . To determine the environmental dose rate, additional material was sampled adjacent to this range. Quartz grains were extracted for  $D_e$  determination, with details on the sample preparation being provided in Sect. S2.2. Each aliquot, with 2 mm silicone stamps, was tested for feldspar contamination using an IRSL stimulation incorporated into the SAR cycle. The overall performance of the measurement parameters was investigated by dose recovery tests, with delivery recovery ratios being 10 % within unity. For all samples but W1-180 (too little material), 40 replicate measurements were carried out for  $D_e$  determination. Several samples show indications of differential bleaching in the form of positively skewed  $D_e$  distributions and large overdispersion values (Table 1, Fig. 2). All luminescence measurements show a relatively low number of initial counts yet provide a clear signal (Fig. 2D). While the Central Age Model was calculated for all samples (CAM; Galbraith et al., 1999), additionally, a Minimum Age Model (MAM; Galbraith et al., 1999) was applied for samples with an overdispersion >20 % and a positively skewed  $D_e$  distribution, which is common for incomplete bleaching of material from a proximal fluvial setting (Table 1). The issue of differential bleaching of fluvial sediments (e.g. Wallinga, 2002; Jain et al., 2004) for determination of the depositional chronology is solved using the MAM (Sect. 5.2).

Determination of the dose rate  $(D_0)$  occurred in the Helmholtz Zentrum Rossendorf laboratory, Dresden, Germany, using gamma spectroscopy. Further details on the sample preparation, estimation of cosmic dose rates, and calculations of the dose rate and ages are provided in Sect. S2.3. In addition, the  $L_{\rm n}/T_{\rm n}$  ratio from IRSL screening allowed

**Table 1.** Dosimetry data and OSL ages of the main cores (coordinates in Table S1). Water content estimation is used for dose rate calculation. MAM ages are preferred over CAM ages for samples with an overdispersion > 20 %.

Sample ID	Uranium (ppm)	Thorium (ppm)	Potassium (%)	Cosmic dose rate (Gy ka <sup>-1</sup> )	Water cont. estimated (%)	Dose rate $(D_0)$ $(Gy ka^{-1})$	Equivalent dose $(D_e)$ $(Gy)$	Over- dispersion (%)	Age model, aliquot no.	OSL age (ka)
W1-30	$5.39 \pm 0.48$	$17.13 \pm 0.71$	$2.94 \pm 0.22$	$0.23 \pm 0.02$	20 ± 5	$4.49 \pm 0.35$	$0.65 \pm 0.04$	26.9	CAM (36/40)*	$0.15 \pm 0.01$
W1-50	$2.89 \pm 0.24$	$11.93 \pm 0.51$	$2.88 \pm 0.22$	$0.22 \pm 0.02$	20 ± 5	$3.67 \pm 0.50$	$1.83 \pm 0.18$ $1.17 \pm 0.17$	58.6	CAM (38/40) MAM (38/40)	$0.50 \pm 0.05$ $0.32 \pm 0.05$
W1-80	$3.30 \pm 0.32$	$11.56 \pm 0.43$	$2.78 \pm 0.19$	$0.20 \pm 0.02$	20 ± 5	$3.64 \pm 0.30$	$3.43 \pm 0.24$ $2.98 \pm 0.15$	41.7	CAM (39/40) MAM (39/40)	$0.94 \pm 0.08$ $0.82 \pm 0.05$
W1-130	$2.41 \pm 0.24$	$9.25 \pm 0.46$	$3.10 \pm 0.32$	$0.19 \pm 0.02$	20 ± 5	$3.57 \pm 0.32$	$20.11 \pm 1.27$ $17.88 \pm 1.87$	37.7	CAM (34/40) MAM (34/40)*	$5.60 \pm 0.50$ $5.00 \pm 0.60$
W1-180	$2.28 \pm 0.21$	$10.53 \pm 0.43$	$3.32 \pm 0.25$	$0.18 \pm 0.02$	$20 \pm 5$	$3.78 \pm 0.22$	$48.81 \pm 1.58$	14.2	CAM (23/25)	$12.9 \pm 0.8$
W2-50	$4.02 \pm 0.40$	$14.67 \pm 0.57$	$2.78 \pm 0.19$	$0.22 \pm 0.02$	20 ± 5	$3.96 \pm 0.36$	$2.34 \pm 0.19$ $1.64 \pm 0.27$	44.0	CAM (34/40)* MAM (34/40)*	$0.59 \pm 0.05$ $0.41 \pm 0.07$
W2-70	$3.22 \pm 0.40$	$11.27 \pm 0.46$	$2.78 \pm 0.19$	$0.21 \pm 0.02$	20 ± 5	$3.61 \pm 0.24$	$13.37 \pm 0.66$	28.3	CAM (36/40)	$3.70 \pm 0.20$
W2-90	$2.25 \pm 0.24$	$8.82 \pm 0.38$	$2.88 \pm 0.22$	$0.20 \pm 0.02$	20 ± 5	$3.36 \pm 0.22$	$32.73 \pm 1.40$ $30.34 \pm 2.54$	26.2	CAM (40/40) MAM (38/40)*	$9.80 \pm 0.60$ $9.00 \pm 0.90$
W2-130	$1.52 \pm 0.21$	$6.24 \pm 0.27$	$2.66 \pm 0.19$	$0.19 \pm 0.02$	20 ± 5	$2.89 \pm 0.17$	$35.04 \pm 0.96$	15.1	CAM (35/40)*	$12.1 \pm 0.7$
S5-30	$2.65 \pm 0.32$	$10.41 \pm 0.43$	$2.66 \pm 0.19$	$0.23 \pm 0.02$	20 ± 5	$3.40 \pm 0.38$	$0.64 \pm 0.07$ $0.40 \pm 0.06$	60.2	CAM (41/45) MAM	$0.19 \pm 0.02$ $0.12 \pm 0.02$
S5-50	$2.57 \pm 0.40$	$9.71 \pm 0.51$	$2.63 \pm 0.25$	$0.22 \pm 0.02$	20 ± 5	$3.29 \pm 0.33$	$2.71 \pm 0.23$ $1.22 \pm 0.16$	53.8	CAM (44/45) MAM	$0.83 \pm 0.09$ $0.37 \pm 0.05$
S5-80	$1.74 \pm 0.20$	$7.24 \pm 0.32$	$2.44 \pm 0.19$	$0.20 \pm 0.02$	20 ± 5	$2.83 \pm 0.17$	$11.07 \pm 0.38$	19.5	CAM (38/40)*	$3.90 \pm 0.20$
S5-130	$1.24 \pm 0.16$	$4.27 \pm 0.19$	$2.09 \pm 0.16$	$0.19 \pm 0.02$	20±5	$2.29 \pm 0.14$	$9.62 \pm 0.28$	15.1	CAM (37/40)*	$4.20 \pm 0.30$

<sup>\*</sup> Outliers have been removed.

us to gain rough age estimations for non-luminescence-dated cores by means of the approximated  $D_e$  and an estimated  $D_0$  per sample.  $D_0$  is largely dependent on the concentration of radioactive elements, which depends considerably on the grain size of the material. The highest correlation between the  $D_0$  of OSL samples and grain size components exists for the mean grain size ( $M_Z$ ). Linear regression then derived the IRSL  $D_0$ . Ultimately, ages and errors were approximated and were carefully interpreted for geochronology of the IRSL-screened cores. As the  $D_0$  was given a 50 % uncertainty and because the ages are computed as the palaeodose divided by the dose rate, these approximated IRSL ages have asymmetrical error bars.

Additionally, four radiocarbon samples were recovered from the cores. Further details on the sample preparation are provided in Sect. S2.4. The samples were handled by the Vilnius Radiocarbon Laboratory, Lithuania. Radiocarbon ages (<sup>14</sup>C yr BP relative to the year 1950) were calibrated with the OxCal v. 4.4 (Bronk Ramsey, 2009) program using the Int-Cal20 calibration curve (Reimer et al., 2020).

Sedimentation rates of the Kinzig floodplains were determined for the three main cores based on the OSL dates (Sect. 4.1). Using propagation of uncertainties in the luminescence ages, error ranges of the sedimentation rates were calculated (Sect. S2.5). However, determining average depo-

sition rates is affected by locally varying factors such as lags in anthropogenically triggered enhanced sedimentation (sediment cascade concept; Trimble, 1999), as well as the local anthropogenic landscape impact (e.g. Lang and Honscheidt, 1999; Lang, 2003; Rommens et al., 2006; Fuchs et al., 2010; Larsen et al., 2013; Verstraeten et al., 2017). Even though derived sedimentation rates may not represent quantitative catchment-scale changes, they can be interpreted by describing overall trends. Namely, it is expected that a shared direction and magnitude of change in sedimentation rates at different sites is not a coincidence. Further details on the computation and uncertainties of sedimentation rates are provided in Sect. S2.5.

# 3.5 Geophysical exploration

Along the drilling transects, electrical resistivity tomography (ERT) and ground-penetrating radar (GPR) measurements were carried out to augment the subsurface information obtained from percussion drillings and hand augerings and to facilitate stratigraphic interpretation. ERT measurements used a SYSCAL Pro resistivity meter with 48 electrodes distributed across two cables in a Wenner array. The electrodes were spaced at a minimum of 1 m to ensure sufficient vertical resolution (Loke, 2004), aligning with the study's focus on the upper overbank fines. The ERT survey

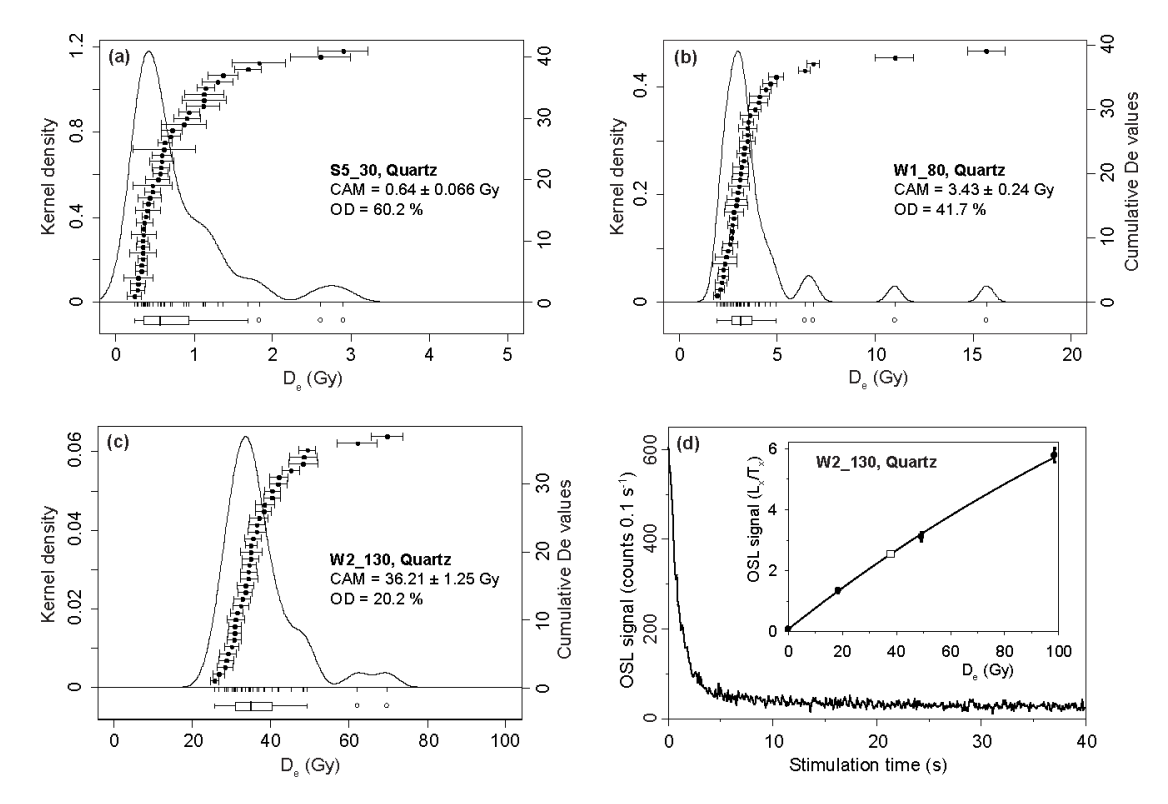


Figure 2. (a–c) Examples of  $D_e$  distributions of three quartz samples of different ages. Note the right-skewed dose distributions of all samples that are typical for partial (differential) bleaching prior to deposition. Boxplots indicate the 1.5 interquartile range; aliquots within the whiskers are accepted in the applied MAM. (d) Example OSL decay curve and dose growth curve (empty square: natural  $L_n/T_n$  and  $D_e$ ). The relatively low luminescence intensity is typical for the samples investigated here.

data were pre-processed using the Prosys III v. 2.11 (IRIS Instruments, 2024) program, checking, among others, the electrode connection; removing outliers; and adding topography data. Inverse modelling was done using RES2DINVx64 v. 4.10.20 (GeoSoftware, 2022) before tomograms were plotted in ResIPy (Blanchy et al., 2020). The aimed-for model fitness was constituted by root-mean-square errors (RMSEs) of between 1 %–5 % and a maximum number of iterations of four to prevent model overfitting on the observed data.

GPR transects were measured using 100 MHz antennae, a 170 ns time window, and a 0.25 m step size with an odometer wheel. The measurements showed high-resolution inhomogeneities in the shallow subsurface, including delineations of stratigraphic layers and, scarcely, the water table. Additional transects were made perpendicular and parallel to the main ones to study the spatial subsurface variability in some floodplain sections. Data pre-processing was conducted with a common set of filters in the EKKO Project v. 5 (Sensors and Software Inc., 2017) program, including a subtract-mean (dewow) filter to remove low-frequency interferences, bandpass frequency to remove noise at the amplitude borders, and background removal to eliminate airwave and groundwave signals. Interpretation was done after manually adjusting the gain function and hyperbolae fitting to determine the depth using the signal velocity. Validation and interpretation of the processed data were achieved using the drillings as a reference.

#### 4 Results

# 4.1 Descriptions of core sedimentology, geochemistry, and chronology

### 4.1.1 Wolfach

## Main percussion drillings

The main sediment core, W1 (Fig. 1F), located on a ridge that is possibly a levee remnant (Fig. 7), reached 1.91 metres below ground level (mb.g.l.) until hitting coarse gravel or rock fragments (broken-off rock pieces), which was felt and heard with the equipment. The lower layers comprise orange-brown sandy gravel to gravelly sand until 1.51 mb.g.l., covered by a yellowish orange-brown sand (1.51–1.46 mb.g.l.) and a gravelly sand layer. This is followed by dark-brown silty sand layers (1.46–0.99 mb.g.l.) and orange-brown sandy silts (0.99–0.78 mb.g.l.), topped by a silty sand (0.78–0.64 mb.g.l.) and silty gravelly sand layer (0.64–0.49 mb.g.l.). Finally, these layers are covered by brown to light-brown silty sand (up from 0.49 mb.g.l.; Fig. 3). The OM and carbonate values are relatively high

(5.0 wt % and 1.0 wt % at 1 m b.g.l.) with increasing carbonate in the upper 0.30 m b.g.l. and peaking OM in the topsoil with 13.2 wt %.

Barium (Ba) concentrations are lowest (431 mg kg<sup>-1</sup>) at 1.50 mb.g.l., increasing to 634–714 mg kg<sup>-1</sup> (1.04–0.51 mb.g.l.) in the profile and peaking at 1778–1997 mg kg<sup>-1</sup> in the upper 0.5 mb.g.l. Lead (Pb) and copper (Cu) also show an increasing trend but at a lower level (Pb: 28–212 mg kg<sup>-1</sup>; Cu: 6–125 mg kg<sup>-1</sup>), possibly showing a peak by pushed-down material with insertion of a new drill core. The geochemistry shows a shift from a gradual to a strong increase in concentrations from below to above 1 mb.g.l. (Fig. 7).

The five OSL ages for core W1 are in stratigraphical order and place floodplain deposition between  $12.9\pm0.80\,\mathrm{ka}$  (1.72 m b.g.l., W1-180) and  $0.15\pm0.01\,\mathrm{ka}$  (0.14 m b.g.l., W1-30; Table 1). Sedimentation rates derived from these ages are  $0.07\pm0.01\,\mathrm{mm\,a^{-1}}$  for the late Pleistocene-early Holocene,  $0.1\pm0.01\,\mathrm{mm\,a^{-1}}$  for the middle to late Holocene, and  $1.5\pm0.44\,\mathrm{mm\,a^{-1}}$  for the modern period (Table 2). The IRSL-screening values indicate slow aggradation in the lower part of the core, followed by one phase of fast accumulation with average  $L_{\rm n}/T_{\rm n}$  values of around 0.18, starting at 0.76 m b.g.l. Approximated IRSL ages are in good agreement with the OSL ages above 0.75 m b.g.l. but overestimate depositional ages below this depth range (Fig. 3).

The main sediment core W2 (Fig. 1F), drilled in a palaeochannel (Fig. 7), reached 1.57 m b.g.l. until hitting coarse gravel or rock fragments. The lowest gravelly sand layer is covered with 0.46 m thick pinkish orange-brown sand, overlain by orange-brown silty sand layers until 0.64 m b.g.l., topped with brown sandy silt and dark-brown silt from 0.18 m b.g.l. to the topsoil (Fig. 3). Gravel found deep in the core was rounded and large ( $d = 3.0 \, \text{cm}$  at 1.50 m b.g.l.,  $d = 2.5 \, \text{cm}$  at 0.78 m b.g.l.), in contrast to subangular gravel between 0.57 and 0.43 m b.g.l. The OM (15.6–4.3 wt%) and carbonate (1.4–1.0 wt%) values at < 1 m b.g.l. are slightly higher than in core W1 and gradually increase to the core top.

Barium concentrations are lowest are the bottom of the core  $(375\,\mathrm{mg\,kg^{-1}})$  and gradually increase to peak at  $0.35\,\mathrm{m\,b.g.l.}$  ( $1180\,\mathrm{mg\,kg^{-1}}$ ), followed by a decreasing concentration of similar magnitude from the surface to the depth of  $0.48\,\mathrm{m\,b.g.l.}$  Lead shows a similar trend, with low values at the core bottom  $(27\,\mathrm{mg\,kg^{-1}})$  and peaking at  $131\,\mathrm{mg\,kg^{-1}}$  ( $0.35\,\mathrm{m\,b.g.l.}$ ). Copper concentrations peak relatively deep in the core, with  $89\,\mathrm{mg\,kg^{-1}}$  ( $1.13\,\mathrm{m\,b.g.l.}$ ), possibly by means of pushed-down material, aside from showing a similar trend compared to Ba and Pb in the upper metre, with elevated concentrations from ca.  $0.62\,\mathrm{m\,b.g.l.}$  upward.

The four OSL ages for W2 are in stratigraphical order and place floodplain deposition between  $12.1 \pm 0.70 \,\mathrm{ka}$  (1.24 m b.g.l., W2-130) and  $0.41 \pm 0.07 \,\mathrm{ka}$  (0.35 m b.g.l., W1-50; Table 1). Sedimentation rates derived from these ages are  $0.1 \pm 0.04 \,\mathrm{mm \, a^{-1}}$  for the late Pleistocene–early

Holocene,  $0.07\pm0.01~\mathrm{mm\,a^{-1}}$  for the middle to late Holocene, and  $0.8\pm0.14~\mathrm{mm\,a^{-1}}$  for the modern period (Table 2). The IRSL-screening values indicate slow aggradation in the lower part of the core, followed by a phase of initial rapid accumulation (average  $L_{\rm n}/T_{\rm n}$  values 0.66 over 0.75–0.48 m b.g.l.) and, finally, more stable fast accumulation, with average  $L_{\rm n}/T_{\rm n}$  values of around 0.18. Approximated IRSL ages appear to be in good agreement with the OSL ages between 1.25 and 0.60 m b.g.l. but overestimate depositional ages closer to the surface (Fig. 3).

### Other cores

Overall, the other cores follow the stratigraphy described above, although these lack sand layers. Gravel deposits (mainly > 1.23 m b.g.l.) in core W3 (palaeochannel closer to the channel; Figs. 7 and S3) are primarily rounded and are at similar depths as in core W1 (gravel layer 0.60-0.55 m b.g.l.). However, these are less angular than those in core W4 (closer to the current channel), with a gravel layer starting at 0.93 mb.g.l. (Figs. 4 and 7). The topsoil OM and carbonate contents of core W4 are 30 %-41 % lower than cores W1 and W2, likely due to the location outside the main agricultural meadow. A common agricultural practice of applying ground limestone on agricultural fields could cause relatively low contents on the path adjacent to the meadow (comparing cores W1 and W2 with core W4). Additionally, the topsoil (0.02-0.11 m b.g.l.) barium concentrations in core W4 (727–807 mg kg $^{-1}$ ) agree with the shallowest  $(0.74 \,\mathrm{m}\,\mathrm{b.g.l.})$  core W2 concentration  $(975 \,\mathrm{mg}\,\mathrm{kg}^{-1})$ , as do the lead and copper concentrations. The  $L_n/T_n$  spread is high throughout core W3, with generally higher values than in the main cores. Contrastingly, in core W4, the  $L_{\rm n}/T_{\rm n}$  values gradually increase upward, like in the main cores, yet increase sharply (0.36–1.17) at shallow depths (0.42 m b.g.l.).

Most hand augerings could not penetrate  $> 1.00 \,\mathrm{m}\,\mathrm{b.g.l.}$ , except for cores Wo16 and Wo17 far up the floodplain, which reached even deeper than the percussion drillings. The stratigraphy follows that of the percussion-drilling cores, with gravelly sands at the bottom covered by silty sands and then topped by sandy silts. The cores reveal pure sand layers at different depths: specifically, the deeper, the further away from the current channel (0.45 mb.g.l. (Wo01); ca. 0.90 m b.g.l. (Wo02, Wo05); ca. 1.10 m b.g.l. (Wo13, Wo16); 1.55 m b.g.l. (Wo15); 1.85 m b.g.l. (Wo17)). Mixtures of angular and rounded gravel ( $d = 0.5-3.0 \,\mathrm{cm}$ ), as well as rock fragments ( $d = 1.0-3.0 \,\mathrm{cm}$ ), increase in frequency at depths > 0.40 m b.g.l. Charcoal fragments were found throughout most cores, and brick fragments were found mainly in sandy silt matrices at increasing depths further away from the current channel, ranging from 0.26 m b.g.l. (Wo07) to 0.72 m b.g.l. (Wo17) over a maximum elevation increase of 0.60 m.

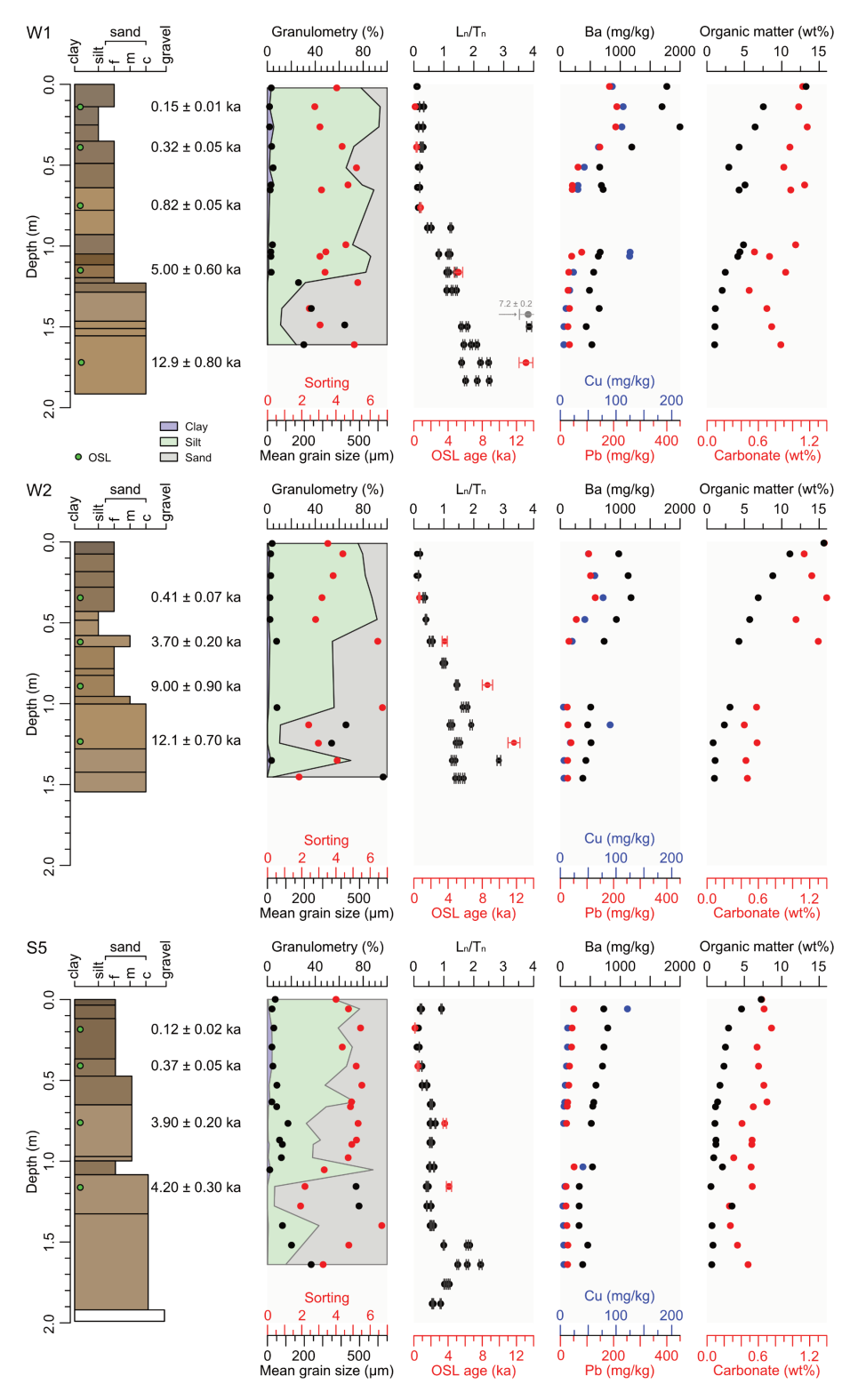
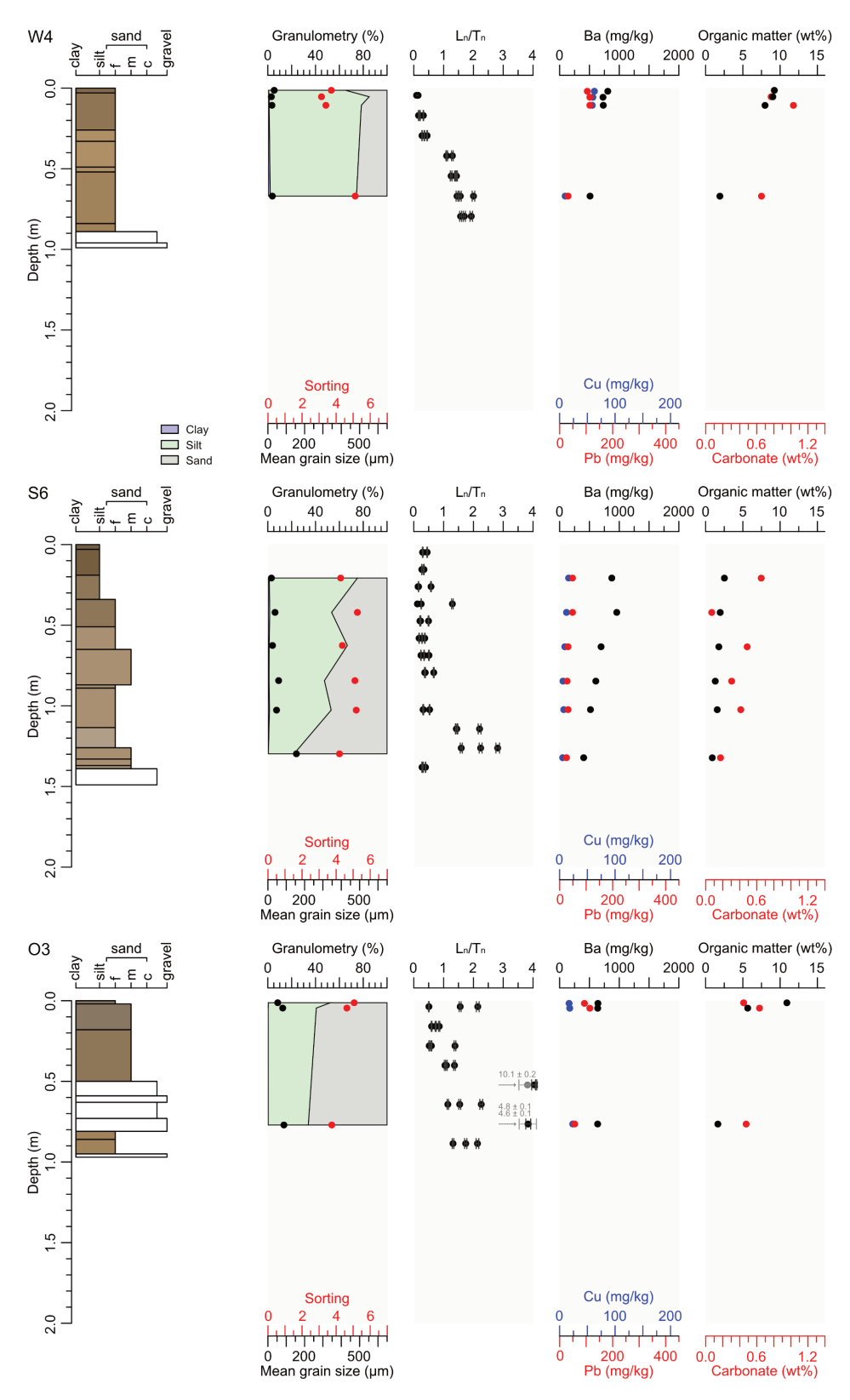


Figure 3. Stratigraphic logs of the main cores, W1, W2 (Wolfach), and S5 (Schenkenzell), including layers shown in Munsell colours and the results of OSL dating. The columns display (from left to right) grain size distributions;  $L_n/T_n$  values (black) and OSL ages (red); concentration of Ba (black), Pb (red), and Cu (blue); and the wt % of both OM and carbonate. The high  $L_n/T_n$  value at 1.39 m depth in W1 likely represents partial bleaching related to a flood event.



**Figure 4.** Stratigraphic logs of the cores W4 (Wolfach), S6 (Schenkenzell), and O3 (Oberwolfach), including layers shown in Munsell colours. The columns display (from left to right) grain size distribution;  $L_{\rm n}/T_{\rm n}$  values (black); concentrations of Ba (black), Pb (red), and Cu (blue); and the wt % of both OM and carbonate. The extreme  $L_{\rm n}/T_{\rm n}$  values at 0.52 and 0.76 m depth in O3 likely represent partial bleaching related to a flood event.

#### 4.1.2 Schenkenzell

# Main percussion drilling

The main sediment core S5 (Fig. 1E) reached 1.99 m b.g.l. until hitting coarse gravel or rock fragments (Fig. 3). The lower layers consist of pinkish-brown sandy gravel and gravelly sand until 1.33 m b.g.l., covered by orange sand and silty sand layers, followed by layers of brown sandy silts from 0.65 m b.g.l. until the topsoil. A gravelly layer (0.65–0.37 m b.g.l.) with angular and rounded gravels underlies the sandy silts. The low OM and carbonate values increase to the top of the core with, relative to the increase in carbonates, high OM values in the upper 0.3 m b.g.l., peaking at 7.3 wt %.

Barium concentrations are lowest at the bottom of the core  $(372 \text{ mg kg}^{-1})$  and gradually increase toward the top, reaching  $704-791 \text{ mg kg}^{-1}$  in the upper 0.5 m b.g.l. Lead and copper show a similar trend but at considerably lower values than barium (Pb  $27-50 \text{ mg kg}^{-1}$ ; Cu  $6-13 \text{ mg kg}^{-1}$ ,  $120 \text{ mg kg}^{-1}$  at 0.06 m b.g.l.). Aside from the increasing trend to the core top, barium values are also elevated at depths of > 1 m b.g.l., and lead values are elevated at depths of > 1 m b.g.l. and increase steadily above. The second metre below the surface possibly shows concentration peaks in the upper layer as a result of pushed-down material.

The four OSL ages for S5 are in stratigraphical order and place floodplain deposition between  $4.20\pm0.30\,\mathrm{ka}$  (1.16 m b.g.l., S5-130) and  $0.12\pm0.02\,\mathrm{ka}$  (0.18 m b.g.l., S5-30; Table 1). Sedimentation rates derived from these ages are  $0.1\pm0.01$  and  $1.3\pm1.56\,\mathrm{mm\,a^{-1}}$  for the middle to late Holocene and increase to between  $0.9\pm0.20$  and  $1.5\pm0.25\,\mathrm{mm\,a^{-1}}$  for the modern period (Table 2). The IRSL-screening values indicate two phases of fast accumulation (stable  $L_{\rm n}/T_{\rm n}$  over depth). The highest average  $L_{\rm n}/T_{\rm n}$  values of 1.83 are close to the bottom (1.64 m b.g.l.), after which the average  $L_{\rm n}/T_{\rm n}$  decreases to 0.51 (1.28–1.04 m b.g.l.) and 0.36 (0.77–0.06 m b.g.l.). Approximated IRSL ages are in good agreement with the OSL ages below 0.5 m b.g.l. but consistently overestimate depositional ages closer to the surface (Fig. 5).

## Other cores

The most southern percussion drilling (S3) reached blackish to pinkish gravelly sand at 1.97 m b.g.l., covered by pinkish-brown silty sand until 0.60 m b.g.l. and followed by light-brown sandy silt to greyish-brown silt to the topsoil (Fig. S3). Core S4 deviates from this with thick sandy gravel layers and generally intermixed gravel throughout most of the profile (Fig. S3). The northernmost core (S6) reached similar depths, with blackish to pinkish sand and silty sand layers between 1.33 and 0.87 m b.g.l., covered by brown sandy silts until the topsoil (Fig. 4). Whereas the OM and  $L_{\rm n}/T_{\rm n}$  values in the other percussion drillings appear to follow those of S5, the carbonate levels are generally over 25 wt % lower

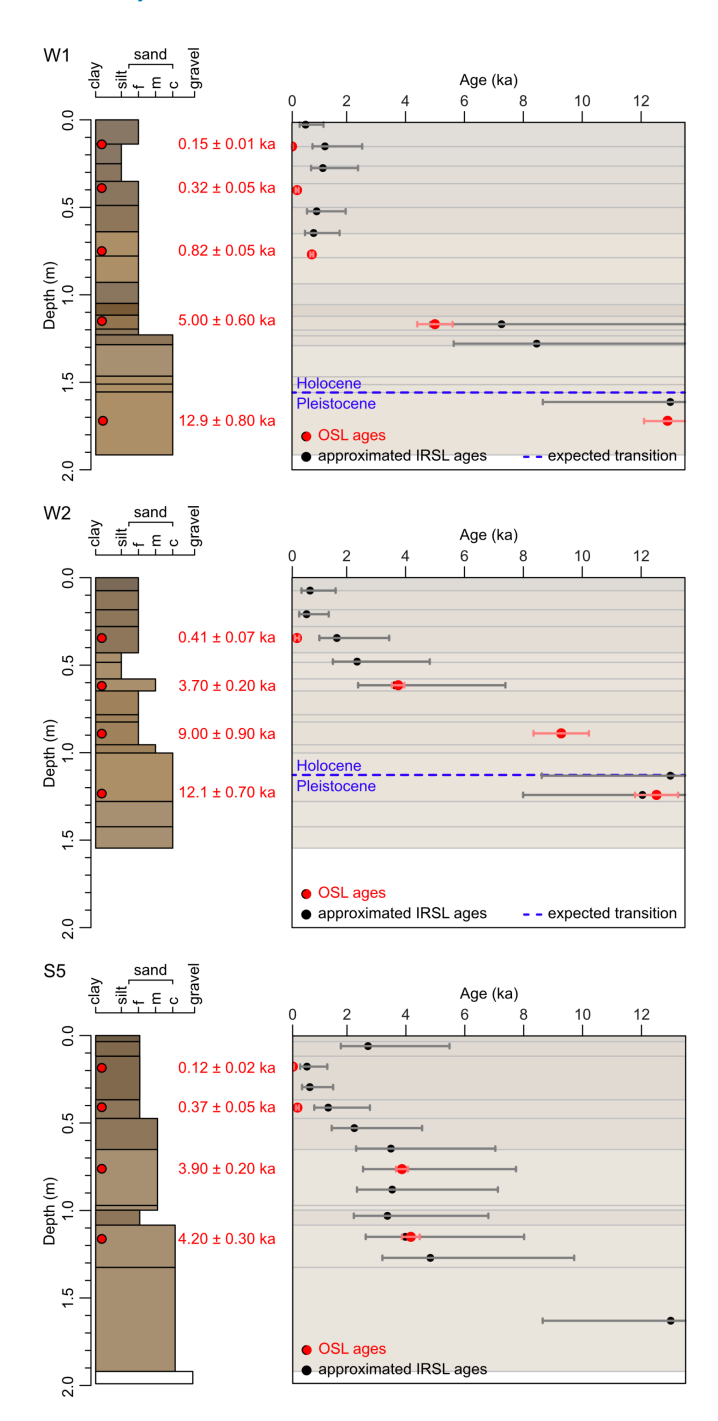


**Figure 5.** Comparison of OSL ages and approximated IRSL ages from screening of the main cores. Error bars of the approximated IRSL ages: 50% of the  $D_0$  uncertainty (details: Sect. 3.4). Backgrounds of the plotting area (age over depth) are the stratigraphic layers taken from Fig. 3. Expected Pleistocene–Holocene transition based on sedimentological descriptions and OSL dating: drawn for interpretation purposes; exact depths are unknown.

throughout the profiles. As the additional cores of the northeastern floodplain section (cores S1 and S2, Fig. 1E) contain poorly sorted (alternating between sandy silt, silty sand,

**Table 2.** Sedimentation rates from main cores and attributed episodes. Late Pleistocene–early Holocene: to 9.0 ka. Middle to late Holocene: 9.0–0.82 ka. Modern: 0.82–0 ka.

Core	Depth range	Segment	Age range	Duration	Sedimentation rate	Episode
	(m)	(mm)	(a)	(a)	$(\text{mm a}^{-1})$	
W1	0.14-0.00	138	150-0	150	$0.92 \pm 0.06$	Modern
W1	0.39-0.14	250	320-150	170	$1.47 \pm 0.44$	Modern
W1	0.76 - 0.39	374	820-320	500	$0.75 \pm 0.11$	Modern
W1	1.16-0.76	400	5000-820	4180	$0.10 \pm 0.01$	Middle to late Holocene
W1	1.72-1.16	559	12 900-5000	7900	$0.07 \pm 0.01$	Late Pleistocene-early Holocene
W2	0.35 - 0.00	345	410-0	410	$0.84 \pm 0.14$	Modern
W2	0.62 - 0.35	270	3700-410	3290	$0.08 \pm 0.01$	Middle to late Holocene
W2	0.89 - 0.62	270	9000-3700	5300	$0.05 \pm 0.01$	Middle to late Holocene
W2	1.24-0.89	357	12 100-9000	3100	$0.12 \pm 0.04$	Late Pleistocene-early Holocene
S5	0.18 – 0.00	177	120-0	120	$1.48 \pm 0.25$	Modern
S5	0.41 - 0.18	236	370-120	250	$0.94 \pm 0.20$	Modern
S5	0.77 - 0.41	354	3900-370	3530	$0.10 \pm 0.01$	Middle to late Holocene
S5	1.16-0.77	390	4200–3900	300	$1.30 \pm 1.56$	Middle to late Holocene

gravel) anthropogenic material (manufactured metal, scraps, bricks, burned printed paper), the study focus shifted to the southern floodplain (Fig. 1E). Here, hand augerings did not reach similar depths as the percussion drillings due to hitting impenetrable gravel layers. Generally, gravelly material was reached between 1.30 and 0.25 mb.g.l., covered with either silty sand or silt at the top. Exceptions to these profiles were peat in a sandy silt matrix in cores Sc09 (1.74–1.50 mb.g.l.), Sc10 (1.59–1.45 m b.g.l.), and Sc18 (0.47 m b.g.l.) (Fig. 7). One peat sample at a depth of 1.57 m b.g.l. (Sc10) was radiocarbon dated to 710 (+60/-40) cal BP (Table S2, Fig. S2). Contrastingly, the other radiocarbon samples (Sc18, Sc13) were dated to be too modern (Table S2, Fig. S2). Additionally, charcoal fragments were generally present in the sandy silt or silty sand deposits, mainly at the northern edge of the meadow. Further north, several boulders (max.  $d = 40 \,\mathrm{cm}$ ) were found close to the surface of drillings Sc18-Sc21 on the slope to the flat topography of the riparian forest (Fig. 7).

#### 4.1.3 Oberwolfach

# Percussion drillings

The percussion drillings (Fig. 1D) reached a maximum depth of 0.97 m b.g.l. until hitting coarse gravel or rock fragments, similarly to the gravel layers in cores O3 and O5 (Figs. 7 and S4). To avoid the colluvial deposits in proximity of the southeastern hillslope, percussion drillings were concentrated in the floodplain section close to the current channel. The cores O4 and O5, furthest away from the channel, consist almost exclusively of brown sandy silt (Figs. S4 and S5). Contrastingly, the core O2 comprises two sand layers (0.43–0.37 m b.g.l.; 0.07–0.00 m b.g.l.) and orange-brown silty sand (Fig. S4). In core O1, a coarsening upward sequence consists of a pinkish-brown sand layer (0.14–0.08 m b.g.l.) covered by a light-brown silty sand layer (Fig. S4). The cen-

trally located core O3 reached 0.97 m b.g.l. (Fig. 7), with gravel covered by an orange-brown silty sand layer until reaching alternating gravel and sandy gravel layers (including fragments of  $d=5\,\mathrm{cm}$ ) between  $0.81-0.50\,\mathrm{m}\,\mathrm{b.g.l.}$ , followed by brown silty sand until reaching a thin brownishgrey sandy silt topsoil. The OM and carbonate content of the topsoil are ca. 5 wt %-8 wt % and 0.4 wt %-0.7 wt %, respectively, with slightly lower carbonate values (< 0.6 wt %) in > 0.50 m b.g.l. of O2.

Barium concentrations are somewhat constant throughout the cores (average O2:  $705 \,\mathrm{mg \, kg^{-1}}$ ; average O3:  $639 \,\mathrm{mg \, kg^{-1}}$ ). Lead has a larger concentration difference between the deepest sample and the average of the upper samples, namely  $61 \,\mathrm{mg \, kg^{-1}}$  relative to  $87 \,\mathrm{mg \, kg^{-1}}$  for O2 and  $57 \,\mathrm{mg \, kg^{-1}}$  relative to  $104 \,\mathrm{mg \, kg^{-1}}$  for O3. The trend for copper follows that of barium closely.

The spread of IRSL-screening  $L_{\rm n}/T_{\rm n}$  values is large, ranging from 0.51 up to 10.10 in core O3 and from 0.09 up to 10.10 between all cores, implying the presence of paterial bleaching and impacting geochronological interpretation of the shallow layers. The  $L_{\rm n}/T_{\rm n}$  values are especially large in the coarse layers of O3, where the matrix contains many small rock fragments.

## Other cores

The hand augerings generally revealed sandy gravelly silt or gravelly silty sand until 0.50 m b.g.l., covered with sandy silts and a thin silty sand topsoil, with the deepest drills located close to the current channel and on top of the hillslope (Fig. 7). The lowest layers include angular and rounded gravel (d = 0.5-1.5 cm at Ob02; d = 3 cm at Ob03) within a moderate to coarse sandy silt matrix. Drillings close to the current channel generally found coarse sand lenses at decreasing depth further away from the channel (0.45 m b.g.l. at Ob04; 0.30 m b.g.l. at Ob06; 0.20 m b.g.l. on the side of a

coarse gravel at Ob07). Drillings on the hillslope often found rock fragments at  $> 0.50 \,\mathrm{m}$  b.g.l., possibly indicating weathered hillslope material covered by fine deposits.

# 4.2 Geophysical investigation and floodplain cross-sections

The derived floodplain cross-sections (Fig. 7) are mainly based on drilling results, supported by ERT (Fig. 8) and GPR findings (Fig. 9). While the top of gravel bodies (Fig. 7) are based on the maximum depths of drillings, ERT results helped in separating fine (silt–sandy silt,  $< 2000 \,\Omega m$ ), medium (silty sand-gravelly sand,  $2000-2100 \Omega m$ ), and coarse (gravelly sand-gravel, 2100-2500 Ωm) sediments (Fig. 8). These stratigraphical units were identified by crossreferencing resistivities from inversions with low root-meansquare errors (RMSEs) (ca. 1.0%) and a limited number of iterations (maximum of four) with the sediment cores. High resistivities are commonly associated with dry and coarse deposits, of which the range in values is regionaland site-specific. The low resistivities close to the floodplain surface are likely to be the result of increased water content (Archie, 1941) following precipitation (23.5 L m<sup>-2</sup>, Deutscher Wetterdienst) that occurred 2 (Wolfach, Oberwolfach) to 3 d (Schenkenzell) before measurement. Unfortunately, the groundwater table is not identifiable everywhere by the ERT or GPR results (Figs. 8 and 9).

#### 4.2.1 Wolfach

Along the Wolfach transect (Fig. 7A), the thickness of finegrained layers increases away from the channel until the transition to a higher floodplain terrace that is flooded less frequently (LUBW, 2024), reflected in the reduced thickness of flood loams in core Wo18. The drillings and geophysical results imply the presence of three palaeochannels by the dipping coarser layers (around Wo05, between Wo09 and Wo10, around Wo16). Silty material was detected with a thickness of only ca. 0.30 m b.g.l. (W4) close to the current channel, relative to 1.85 m b.g.l. (Wo17) at the floodplain edge. Generally, gravelly sandy silts to silty sands are covered by sandy silts floodplain-wide. Interestingly, a constantly thick sand layer close to the channel appears to be non-continuous and at greater depth further away from the channel. Additionally, the sandy gravelly silts point toward former lateral channel migration that intensely reworked sediments. Although the Wolfach site is located ca. 18 km downstream of the Schenkenzell site (Fig. 1C), the overbank fines did not show larger thicknesses.

# 4.2.2 Schenkenzell

The fine overbank deposits in the Schenkenzell floodplain (Fig. 7B) are of varying thickness: at least 1.60 m b.g.l. (Sc09) around the centre compared to 0.50 m b.g.l. (Sc19) in the elevated riparian area. Dipping silty layers indicate flu-

vial structures like palaeochannels or scroll bar deposits that are not always reflected in the stratigraphy of the underlying gravel beds. The exception is two layers of peat in sandy silt matrices at similar depths. These are likely to have formed by OM accumulation in formerly active channels rather than under lacustrine conditions as the silty deposits lack the characteristic well sorting and lamination. Coarse material (moderate to coarse sand, gravel) was detected at a relatively shallow depth in, in particular, the palaeochannel section and slope to the elevated riparian area. Sandy material was generally found ca. 1.0 m below silty material, except for the very shallow presence at Sc12. Finally, pure silt layers were mainly found in the currently present floodplain depressions. East of the palaeochannels, silty sand layers are detected at shallower depths. These, in combination with the poorly sorted deposits along the slope, point toward either strong incision and reworking of the floodplain material removing significant amounts of sandy material or human disturbances by dredging sediments out the palaeochannels that were used, if not made, for timber raft.

#### 4.2.3 Oberwolfach

At the Oberwolfach transect (Fig. 7C), the thickness of overbank fines varies between ca. 0.5 mb.g.l. at the floodplain centre and ca. 1.0-1.5 mb.g.l. at the foot of the hillslope and close to the riverbank. While the thicker accumulation of fines close to the river is likely owed to more frequent sediment input from small floods, increased thickness of finegrained sediments at the foot of the hillslope (Ob12–Ob14) may reflect colluvial sedimentation. Thicker zones of coarse material are indicated by elevated resistivities in the ERT measurements both on the hillslope and in the central part of the floodplain. At the transition from hillslope to floodplain, reduced resistivities point to fine-grained material, and dipping reflectors revealed by the GPR measurements point to a palaeochannel with colluvial fill. The generally thin sediment cover on the floodplain at the most upstream study site at Oberwolfach is likely the result of the small upstream catchment area and the confined floodplain.

#### 5 Discussion

# 5.1 Floodplain architecture

The floodplain architecture of the Kinzig is dominated by a gradual transition from poorly sorted gravel layers at the base of the sediment sequences to fine-grained layers of flood loams close to the surface that indicate a shift in the fluvial regime. The gravel layers at the base of the sediment sequences are likely to be the remnants of Pleistocene braided riverbeds that formed under climatic characteristics of low temperatures with sparse vegetation cover, limited soil formation, and limited precipitation (mainly physical weathering of the crystalline basement; Lang et al., 2003; Erkens et

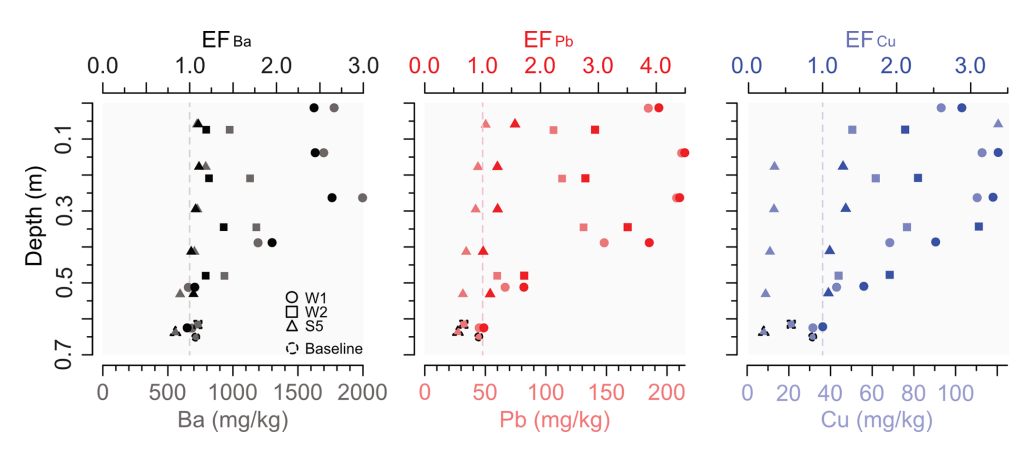


Figure 6. Enrichment factors of Ba, Pb, and Cu (top x axis) over depth for the fine overbank deposits for the main cores (y axis), including the baseline samples per core and element. Concentrations over depth as a reference is shown at the bottom x axis. The Cu peak in the core S5 is excluded (Table S5). The dashed vertical line indicates EF = 1.0 as the baseline.

al., 2009; Abdulkarim et al., 2024). Subsequently, the climatically warmer and wetter Holocene increased the protective vegetation cover and thus stabilised the hillslopes, resulting in decreased physical bedrock weathering and less supply of coarse (bedload) material to the river. Simultaneously, intensified chemical weathering of surface material initiated soil formation and enhanced infiltration of runoff (Rösch, 1989; Bork, 1998; Friedmann, 2000; Mäckel, 2000; Sudhaus and Friedmann, 2006). Ultimately, due to the changed nature of sediments (coarse to fine) and more continuous discharge, the river system likely shifted further from sinuous multiple channels to an increasingly entrenched single-thread channel (classification from Rosgen, 1994). Channels cut into the Pleistocene deposits, while fine-grained sediments were deposited on emerging floodplains and filled-up palaeochannels. One such palaeochannel on the Wolfach floodplain (W2) was last active before  $3.70 \pm 0.20$  ka (Table 1). Floodplain palaeochannels can get abandoned by meander cutoffs, as well as increased sediment delivery (Macklin et al., 2010; Notebaert et al., 2018; Brown et al., 2018). Palaeochannels often have a richness in terms of OM in the upper core layer that is likely to be related to the higher accumulation of OM-binding fine sediments in a relatively low landscape position that simultaneously slows down OM decomposition. The flood loam thicknesses along the Kinzig found in this study (ca. 2.5–0.6 m b.g.l.) is within the 2.0–0.5 m b.g.l. range in other Black Forest valleys such as the Dreisam and Elz catchments (Fig. 1B) (Mäckel, 2000; Seidel, 2004). As for the Kinzig catchment, these thicknesses vary between tributaries of similar dimensions, likely showing different sediment production and sedimentation rates. Namely, overbank deposition occurs via both flood events and hillslopesoil erosion. As this depends on hillslope-channel connectivity and buffer capacity, this contribution varies on small spatial and temporal scales (Dotterweich, 2008). Whereas the hillslope-channel connectivity influences erosion of for-

merly deposited sediments, the buffer function can temporally entrain sediments before remobilisation and further downstream transport.

Within the Kinzig catchment, the thicknesses of overbank fines in further upstream reaches are up to 0.5–0.3 mb.g.l. (Mäckel, 2000) compared to 0.74 mb.g.l. in the Wolf tributary. In contrast, the Elz River (Fig. 1B) has overbank fines of ca. 1.6–0.6 mb.g.l. (Seidel, 2004) that are thicker in downstream locations, i.e. closer to the Upper Rhine Graben. This is likely due to a higher geologic imprint of relatively easily weatherable Buntsandstein, more prevalent loess cover, and earlier human impact (Seidel, 2004).

Aside from these natural processes of floodplain deposition and reworking, the Kinzig floodplains recorded indications of anthropogenic impact in the shape of changed sedimentation rates and geochemical sediment characteristics. In addition to that are the striking loamy to gravelly deposits in the Schenkenzell riparian forest (Sect. 4.1.2 and 4.2.2). These shallow deposits are very poorly sorted (cobbles in silty matrix), as reflected in both the high resistivities on the levee between the two palaeochannels (Sc14,5, Sc15) and the upward slope (Sc18) that were uncovered when drilling (Figs. 7B and 8B). The rounded Buntsandstein cobbles (max. d = 25 cm) could only be transported at high stream power. Whether these were deliberately placed at the channel margin as erosion protection or were exposed by channel incision into Pleistocene gravel layers, as reported by Merz (1987) for the Schiltach Valley, remains unknown. However, as the palaeochannels in this riparian forest were likely used for timber drift and raft (Figs. S11–S13), a land use that requires heavy stream alterations (e.g. channel bed rock clearing), it can be assumed that the dredged material from the natural palaeochannels was moved to adjacent slopes. The anthropogenic impact here might explain the thicker overbank fines relative to the Wolfach floodplain (Fig. 7A and B) as the Schenkenzell site was likely to be actively altered by the tim-

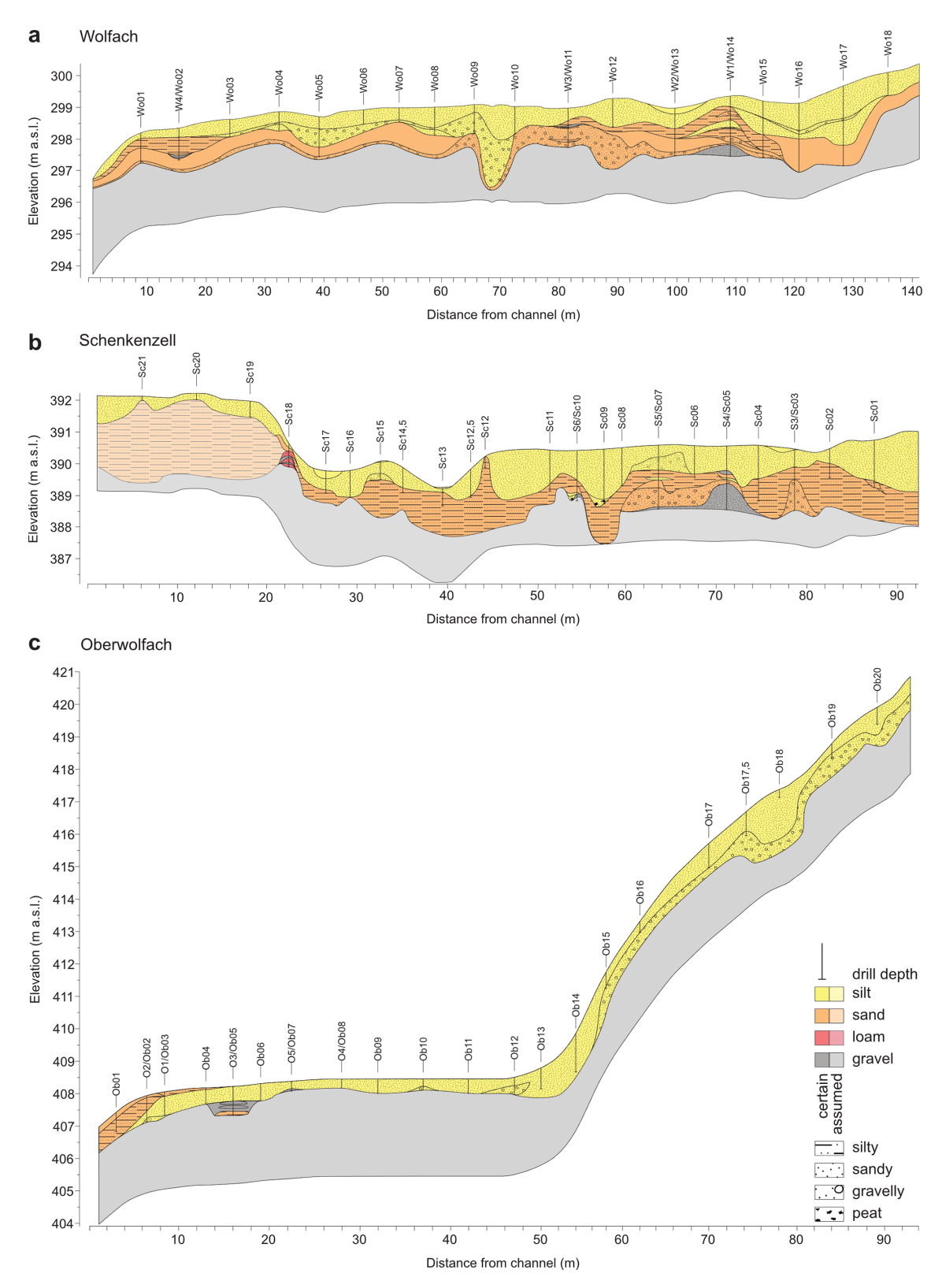


**Figure 7.** Floodplain and hillslope cross-sections with exaggerated elevation profiles (depth over width: factor of 3.6). Primary (colours) and secondary (pattern) sedimentological classes are indicated with a certainty level; vertical lines indicate drilling position and depth.

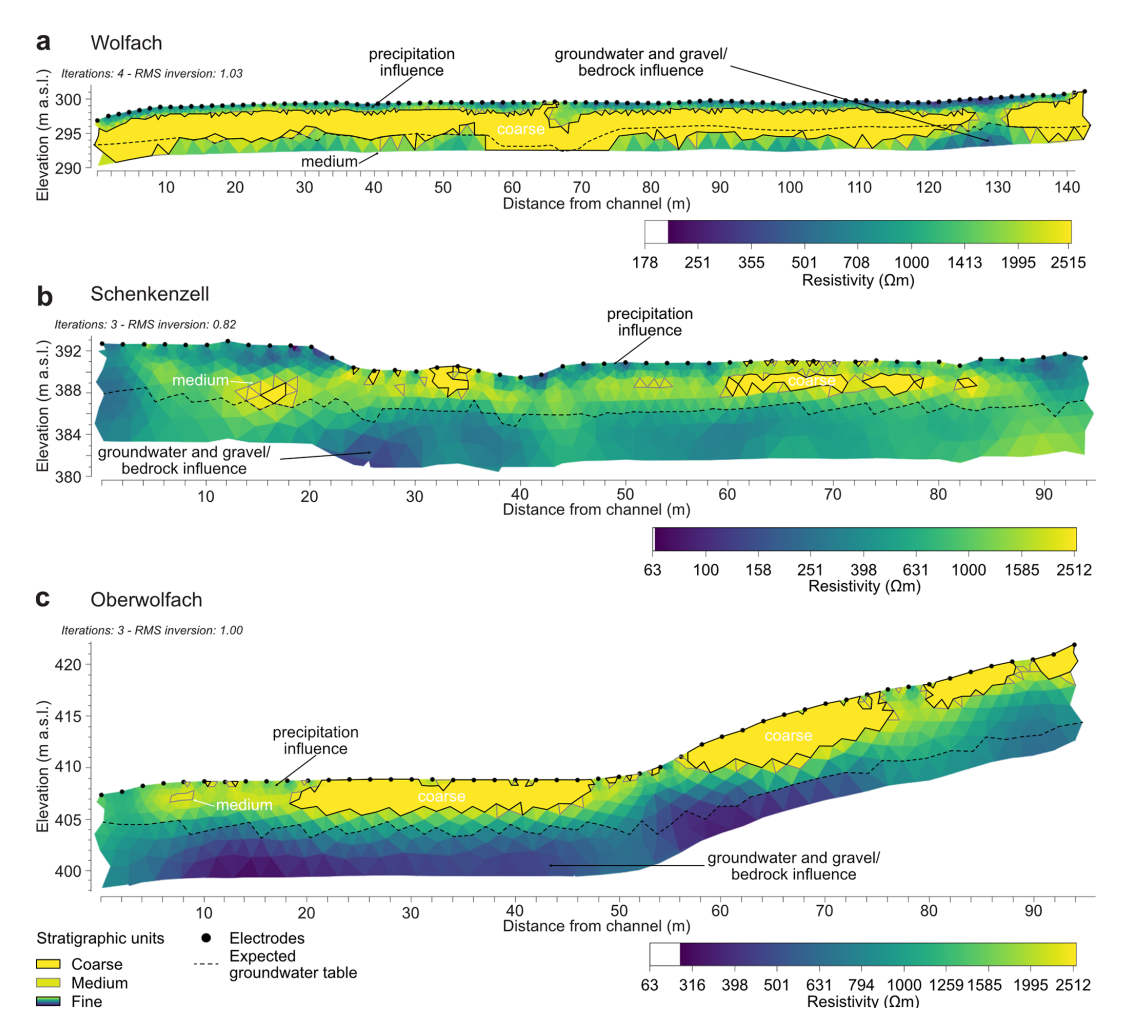


**Figure 8.** Floodplain and hillslope ERT cross-sections, including the stratigraphic units based on cross-referencing with sediment cores. Inversion setting of model refinement in RES2DINVx64 v. 4.10.20 was used to model cells with widths of half the unit (electrode) spacing.

ber drift and raft trade might be an explanation (e.g. binding site, historic weirs, termination of timber transport channel; Figs. 1E and S9–S11). Alternatively, the natural floodplain setting at the Schenkenzell site, where the Kinzig passes through a funnel of a wide to small valley (Fig. 1E), likely induces backwater sedimentation upstream. In comparison, the wider Wolfach floodplain (Fig. 1F) dilutes sediment deposition such that aggrading layers are thinner (e.g. Kanianska et al., 2022; Trimble, 1999), with simultaneous sediment retention (e.g. Belletti et al., 2020) behind an upstream weir in Wolfach with likely anthropogenic channel bifurcation in 1849 CE and behind a modern weir in 1887 CE (Heidelberg, 1849; Braun, 1887).

# 5.2 Depositional chronology and floodplain sedimentation rates

All OSL ages obtained for the cores are in stratigraphical order. While the deepest samples of the cores W1 and W2 reveal deposition during the late Pleistocene, the lowermost

sample from core S5 dates to the Bronze Age. Most (except for two) ages fall into the Holocene period, of which six are younger than 1 ka. Consistently with findings from earlier studies establishing floodplain chronologies in the Upper Rhine Area (Mäckel et al., 2009; Abdulkarim et al., 2024), these OSL ages indicate deposition of poorly sorted gravel layers during the late Pleistocene, followed by a transition from coarse sands to fine-sand- and silt-dominated deposits between the Pleistocene–Holocene transition and the late Holocene.

Supporting the OSL-derived floodplain geochronology is only one out of four radiocarbon dates (core Sc10, ca. 9 m north of core S5) as the other samples (from cores W1, Sc13, and Sc18) likely represent contamination by modern wood, including roots (Table S2, Fig. S2, Sect. S2.4). The dated peat from an abandoned channel at Schenkenzell yields a radiocarbon age of 710 +60/-40 cal BP (Sc10, 1.57 m b.g.l.; Table S2), indicating active floodplain dynamics, namely likely

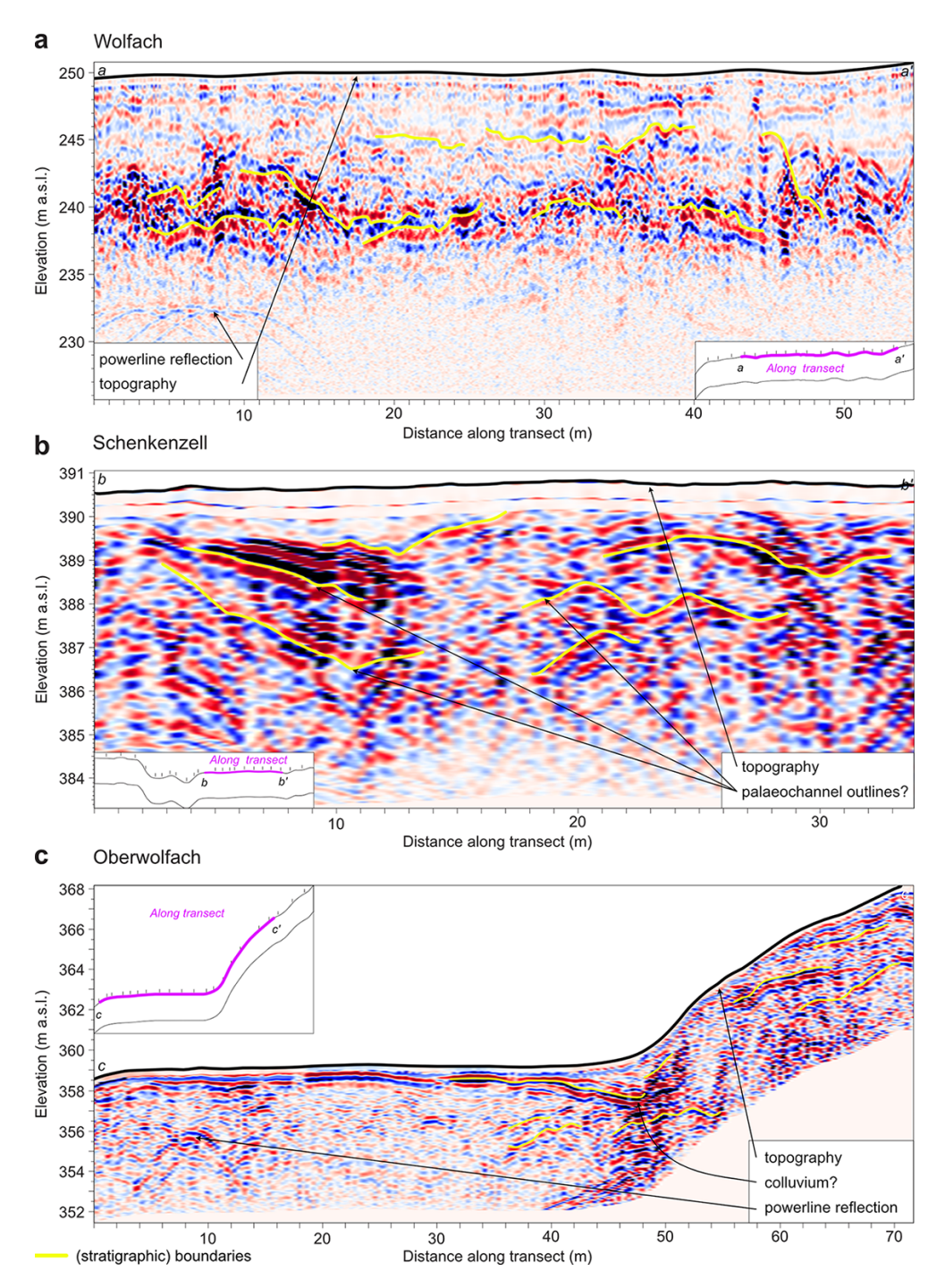


**Figure 9.** Floodplain and hillslope GPR cross-sections after data processing in EKKO Project v. 5. Settings: frequency – 100 MHz; gain or filter – Dewow+SEC2 gain; saturation – 100 %; contrast – 25 %; background subtraction (filter width (m) of 1.5). Insets indicate the position of GPR survey along the floodplain cross-section (Fig. 7).

channel abandonment resulting from lateral mobility in Medieval times.

Approximated IRSL (Table S3) and dated OSL ages (Table 1) roughly align in the main cores, especially for material older than ca. 1 ka (Fig. 5). Here, the age approximations appear to be robust over this dating range. In contrast, the IRSL

age approximations all overestimate the time since deposition for samples dated younger than ca. 1 ka, up to a factor of 9 (Sect. 4.1.3). It is especially apparent in the non-OSL dated cores where the IRSL age approximations are higher over similar depths and types of deposits compared to the main cores (Figs. 4 and S3–S5). The overestimations likely re-

sult from insufficient bleaching of IRSL signals during flood events. It must be noted that the IRSL approach used here does not allow us to correct for the effect of partial bleaching in contrast to proper OSL dating. However, despite its limitations, the approximated IRSL ages allow for roughly identifying depositional episodes and revealing lateral differences in depositional ages (e.g. W2 and W3; Table S3).

The sedimentation rates of the Kinzig floodplains are low (0.1 mm a<sup>-1</sup>) around the Pleistocene-Holocene transition and rise  $(1.1 \text{ mm a}^{-1})$  in modern times but show variability between the study sites (Table 2). Sedimentation rates are relatively stable up to halfway through the Subboreal period  $(0.07 \pm 0.01 - 0.1 \pm 0.01 \text{ mm a}^{-1}, \text{Wolfach};$  $0.1 \pm 0.01$ – $1.3 \pm 1.56$  mm a<sup>-1</sup>, Schenkenzell), which is followed by a roughly simultaneous increase in all cores. From ca.  $0.37 \pm 0.05$  ka (S5), the sedimentation rates increase sharply, up to maximum values of  $1.5 \text{ mm a}^{-1}$  (W1, S5), and then decrease again until the present for W2  $(0.8 \,\mathrm{mm}\,\mathrm{a}^{-1})$ . The sedimentation rates of the three episodes in core W1 of Wolfach are within the range of rates of core W2, and, when computing weighted averages for the episodes by duration, these are slightly higher for the modern period and for the middle to late Holocene (Table 2). Overall, sedimentation rates increased compared to the late Pleistocene-early Holocene  $(0.1 \text{ mm a}^{-1})$  by a factor of 3 during the middle to late Holocene (0.3 mm a<sup>-1</sup>) and by a factor of 11 during modern times  $(1.1 \text{ mm a}^{-1})$ . In comparison, sedimentation rates for the upper ca. 2 m b.g.l. remain below 1 mm  $a^{-1}$ in the neighbouring Elz and Möhlin catchments (Fig. 1B). Here, the sedimentation rates are a factor of approximately 0.6 lower than in the Kinzig, whereas deeper sediments until 2.5 m b.g.l. were deposited with rates of 1.3-3.2 mm a<sup>-1</sup> (Fig. 12) (Mäckel et al., 1996; Mäckel et al., 2002; Mäckel et al., 2003). Further, the Dreisam River (Fig. 1B) has shallower overbank fines than the Kinzig at 0.55-0.35 m b.g.l. at a downstream site (Mäckel and Thomas, 2009), which is likely due to the smaller and wider Dreisam catchment. Moreover, the Möhlin River (Fig. 1B) has similar overbank fine thicknesses but lower sedimentation rates than the Kinzig (Table 2), namely ca.  $0.6 \,\mathrm{mm}\,\mathrm{a}^{-1}$  (to  $1.90 \,\mathrm{m}\,\mathrm{b.g.l.}$ ; Fig. 12) (Seidel, 2004). Here, gravel bodies that are likely to be of similar composition are detected deeper (1.5–1.0 m b.g.l.) compared to along the Kinzig (0.56 m b.g.l., Schenkenzell; 0.65 m b.g.l., Oberwolfach; 0.76 m b.g.l., Wolfach) (Mäckel et al., 1996; Seidel, 2004). With respect to a compilation of sedimentation rates from tributaries of the Rhine catchment in Germany (Hoffmann et al., 2007b), the modern Kinzig sedimentation rates remain in the lower reported range (extremes exceed 5 mm a<sup>-1</sup>). It must be noted, however, that the different catchment scales complied in Hoffmann et al. (2007b) have varying hillslope-channel connectivities and buffer capacities in terms of anthropogenic land use impact relative to the meso-scale Kinzig catchment (Dotterweich, 2008).

One pathway introducing sediment into the river system and resulting in floodplain deposition (lateral linkage as discussed in Fryirs, 2013) is soil erosion. Even though soil erosion cannot be directly linked to floodplain deposition, elevated soil erosion rates reported by several studies for Medieval times in central Europe (e.g. Bork, 1998; Lang et al., 2003; Houben et al., 2006; Dotterweich, 2008; Mäckel et al., 2009; Notebaert et al., 2011) temporally coincide with increased floodplain deposition during periods of increasing anthropogenic land use (Fryirs, 2013). Alternatively, shorter phases of climatic impact, such as the Little Ice Age (LIA, period 1550-1850 CE; Glaser and Riemann, 2009), are likely to have increased coarse-grained overbank deposition and strong lateral erosion in catchments such as the Kinzig (e.g. von Suchodoletz et al., 2024). Additionally, anthropogenic impact is likely to be reflected in intense accumulation phases of the Möhlin and Dreisam rivers (Figs. 1B and 10) that coincide with the regional onset of human settlement (Mäckel and Metz, 1992; Mäckel et al., 1996). These trends agree with the modern deposits along the Kinzig, with high sedimentation rates and the onset of elevated heavy metal content, dated to  $0.37 \pm 0.05$  ka (S5) and  $0.41 \pm 0.07$  ka (W2) (Fig. 3, Table 1).

## 5.3 Heavy metal concentrations

Another proxy of anthropogenic impact on the fluvial system is the concentration of heavy metals in overbank fines that reflect historic ore mining and processing. Celtic small-scale mining likely occurred in the Kinzig catchment from the Bronze Age onward, with the first reliable mining evidence (ore smelting sites) dated between 225 BCE and 165 CE, whereas the Medieval ore-mining rights were first granted in the 11th century (e.g. Riezler, 1877; Knausenberger, 2001; Markl, 2016). Mining intensity peaks (Sect. 2.3) were followed by phases of decreased activity in modern times (excluding prospections in the 20th century), as is likely to be reflected in the decreased Cu and Pb concentrations in Wolfach (W1, W2). Even though barium was not a targeted element, it was common due to the barite-rich veins associated with Ag-Pb-Zn (Zn: zinc) ores in the catchment and therefore functioned as an indicator of mining intensity, with barium concentrations largely exceeding measurement detection limits (e.g. Bliedtner and Martin, 1986).

Describing the heavy element trends relative to other core characteristics with the PCA, the strongest linear correlation explains much of the heavy element variability but not all, being interdependent. Namely, for all study sites, the PCA points to a strong linear correlation with OM contents and major element oxide concentrations (Sects. 5.3 and S4.5). Additionally, the different organic matter contents introduce variability into structural water contents, complicating PCA interpretations. Nonetheless, the positive correlation with organics indicates the heavy metal absorption pathway to organic complexes, whereas the negative correlation with ma-

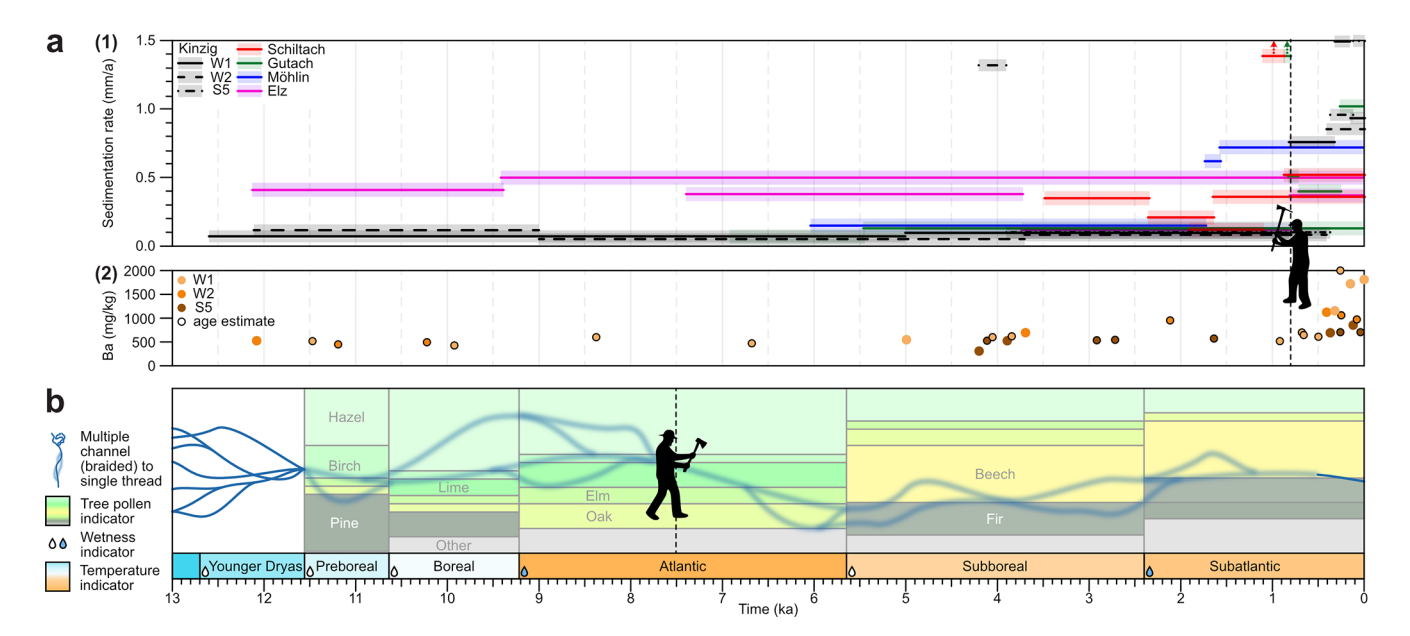


**Figure 10.** Conceptual model of the Kinzig floodplain and regional fluvial development. (a) Local (Kinzig). Top (Kinzig, neighbouring catchments): sedimentation rates in the main cores compared to those from Rhenian Black Forest rivers (two rates > 1.5 mm a<sup>-1</sup>) based on radiocarbon dates. Transparent colour-coded boxes to support identification of rivers. Bottom (Kinzig): Ba concentrations, including values estimated in time based on linear interpolation between the sediment depth and age. Anthropogenic impact: first documented Medieval mining rights (mining indication) from Riezler (1877). (b) Regional (Upper Rhine area). Timeline of environmental conditions in the Upper Rhine area, including river pattern transition (transition phase blurred) and period-averaged tree pollen ratios from the northeastern Elz catchment (Friedmann, 2002). Anthropogenic impact: human presence (deforestation indication) from Lang et al. (2003).

jor element oxides (mainly SiO<sub>2</sub>) hints at lower heavy element concentrations in sandier samples, fitting the preferential heavy element absorption to fine-grained sediments.

One rather simplified consideration of element contaminations is a comparison with regionally derived background values relative to the upper soil of agricultural land or parent material (granite, gneiss; Bodenschutz, 2017). Median concentrations of the Kinzig sediments mostly exceed these background values for samples < 1 m b.g.l. (Wolfach: factor of 4–17 (Cu) and 3–8 (Pb); Schenkenzell: factor of 3–6 (Cu) and 2 (Pb)). These exceedances likely result from the floodplain setting where, naturally, contaminants accumulate with flood loams (e.g. Szabó et al., 2020), which is not considered by the background values of the upper soil of agricultural land that likely only consider agricultural heavy metal inputs such as from fertilisers and pesticides (e.g. cadmium (Cd), Pb, Cu, Zn).

Another consideration is the computation of EFs that require a suitable reference element, found to be V (Sect. S4.4). Leaching of heavy metals within soil columns of the Kinzig floodplain was considered by measuring the topsoil pH in water, finding values within the low-leaching range for cations (5.26–6.22; average: Wolfach – 6.00 and Schenkenzell – 5.79) (Sloot and Kosson, 2010). Ultimately, the EFs show that all upper core sections have elevated heavy metal values, including between- and within-core variations (Fig. 6, Table S5). In particular, the W1 core had the high-

est EFs, being a factor ca. 1–1.5 higher than W2 and 2.5–4 higher than S5 (mostly EFs around 1.0, except for Cu). A consistent EF increase is found at ca. 0.55 m b.g.l., roughly coinciding with decreasing sand and increasing OM contents.

Neighbouring catchments of the Möhlin and Sulzbach rivers, both draining from the southern Black Forest toward the Upper Rhine (Fig. 1B), were historically mined for Ag and Pb and show similar increases in heavy metal concentrations in floodplain sediments (i.e.  $39-1316 \,\mathrm{mg \, kg^{-1}}$ , Pb) as the Kinzig, with the highest concentrations in the silty floodplain sediment deposits (Foellmer, 1999). In these two catchments, natural background values were based on Pleistocene deposits, as well as Holocene deposits from unmined areas. Generally, the heavy metal concentrations peak just below the subsurface in all three catchments before decreasing toward their natural background values, as along the Kinzig. Interestingly, average values for Ba, Cu, and Pb at Wolfach decrease closer to the current channel (exception: W4), whereas Ba and Pb values increase in Schenkenzell. Ultimately, heavy metal peaks were interpreted by Foellmer (1999) as High Middle Ages deposits, which would comply with the W1 and S5 Kinzig cores and likely with the core W2 when considering mixing of the topsoil material by, for example, floods, bioturbation, and ploughing. In the Kinzig catchment, the peaks in elevated heavy metal concentrations coincide with the recorded mining and ore-smelting activity that intensified from the 11th century onward (Fig. 10). Nonetheless, the earliest mining already occurred much earlier, with the first sediments showing elevated heavy metal concentrations in the Kinzig, likely deposited between the Bronze Age and (Early) modern period. Although the exact onset of elevated heavy metal concentrations remains unknown, the chronology points to after 3.9 to 3.7 ka for W2 and S5 (W2–70, S5–80), pointing toward (pre-)Medieval mining, and after 0.82 ka for W1 (W1–80; Table 1).

## 5.4 Natural to anthropogenic fluvial transition

Despite the delayed response of floodplains to increasing anthropogenic impact within the catchment (Verstraeten et al., 2017), an increase in overbank deposition has been documented by several studies (e.g. Lang et al., 2003; Mäckel, 2000; Broothaerts et al., 2014; Brown et al., 2018). Specifically, the direction and magnitude of the floodplain response follow those of anthropogenic catchment disturbances (Verstraeten et al., 2017). However, the onset of enhanced sedimentation rates of the Kinzig, rising from 0.1 to 1.1 mm  $a^{-1}$ (Sect. 4.1), will not directly reflect the onset of anthropogenic catchment land use. Instead, this is likely to indicate its impact on the floodplain sediment delivery as a result of reduced protective soil cover and root system stability on slopes, floodplains, and riverbanks (e.g. Pennock et al., 2019; Brown et al., 2018). Consequently, enhanced hillslope instability and erosivity of fine-grained material enriched streams with higher suspended loads that are partially deposited on the floodplains. Additionally, natural changes in land cover took place simultaneously with anthropogenic impact. This includes changes in the natural forest cover (Mathewes, 2023), though the onset of strong deforestation during the Bronze and pre-Roman Iron Age (Rösch, 2015) was a considerable direct anthropogenic impact. Anthropogenic land use impacts in catchments both directly and indirectly influence floodplain deposition that can be reflected in sedimentation rates that are spatially variable within catchments and floodplains yet still contribute to identifying shifts in the hydrological and sedimentological regimes.

After the Pleistocene–Holocene transition, the patterns of major rivers changed from braided to anabranching and anastomosing in temperate Europe (Brown et al., 2018). The first Kinzig floodplains were likely to be covered with tundratype plant species that made way at the start of the warmer and wetter Atlantic periods with the increased spread of woodland and decreased erosion rates in the Black Forest (e.g. Mäckel and Friedmann, 1999; Mäckel, 2000; Mäckel et al., 2002; Sudhaus and Friedmann, 2006). Pollen data from a raised bog in the northeastern Elz catchment (Fig. 1B) indicate that the mixed oak forest got increasingly outcompeted by a beech fir forest from the Atlantic into the Subboreal (Friedmann, 2002). The Rhine system – and, in all likelihood, its tributaries, such as the Kinzig – experienced stable geomorphic conditions between 8000 and 5500 BCE

(Hoffmann et al., 2008). Then, increased overbank deposition started with the onset of human activity during the Neolithic (ca. 4500 to 1700 BCE), the impact of which increased in various forms from the Neolithic onward (e.g. Hoffmann et al., 2007a; Hoffmann et al., 2008; Lang et al., 2003; Dix et al., 2005). The forest tree species composition changed with the first forest clearings, starting with mainly fir and some beech and oak, and agricultural land use (Friedmann, 2002). The Kinzig catchment underwent agricultural land use, charcoal production, and tanneries (resulting in, for example, deforestation and contaminations), timber drift and raft (e.g. deforestation, channel modifications, discharge alterations), and mining (e.g. deforestation, contaminations). In particular, forest clearance directly impacted fluvial and sediment dynamics (Sect. 5.1), as reflected in increased regional overbank deposition since the Bronze Age (ca. 3200 to 900 BCE), and this was later enhanced by floodplain deforestation during the Iron Age (ca. 1200 to 550 BCE) and the Roman period (Dix et al., 2005; Hoffmann et al., 2007b). Further floodplain management (flattening, drying) in the region resulted in floodplain channels filling up with fines and enhanced floodplain aggradation (Dix et al., 2005). Then, a widespread increase in geomorphodynamic activity in the Rhine system between 1350 to 830 BCE was likely to have been anthropogenically induced (Hoffmann et al., 2008; Friedmann, 2002). The increased silt fractions of the main Kinzig cores around this time possibly reflect this increased pressure of anthropogenic land use (Fig. 3). Supporting this is the roughly simultaneous onset of enhanced heavy metal concentrations in the Kinzig floodplains with population increases during the La Tène period (450-0 BCE) (Mäckel, 2000) and the relatively stable and high sedimentation rates of the main cores (Figs. 3 and 10). The high sedimentation rates on the Kinzig floodplains indicate geomorphodynamic activity that is likely to be related to an increasing human impact as reported by Mäckel (2000) for the Schiltach tributary. Finally, the impact of the wetter and cooler LIA climate was recorded in Rhine sediments (Lang et al., 2003) yet was not detected in the Kinzig cores, possibly due to the limited measurement resolution. Alluvial sedimentation in the Rhine tributaries was therefore likely to be the result of land use changes in the catchments since human occupation (Lang et al., 2003).

Summarising, the morphodynamical history of the Kinzig River – the arguments for which are conceptually illustrated in Fig. 10 – starts with the gravels deposited by a Pleistocene braided system in sparsely vegetated valleys that are currently located ca. 0.6 m (upstream) to 1.6 m (downstream) below the surface. The climatic transition into the Holocene possibly lead to a single-thread river channel with floodplain formation reflecting the changed catchment weatherability and related fine sediment availability. Namely, the fluvial system adaptation is reflected in the gradual floodplain deposit transition into sandy and, later, silty sediments closer to the surface, the studied deposits of which are ambiguous with

regard to proving an anastomosing or anabranching transitional system. After a relatively stable geomorphodynamic phase until ca. 0.82 ka, the Kinzig floodplains changed again with the intensification of anthropogenic activities in the upstream catchment areas. These triggered an enhanced influx of silty material and higher OM contents and heavy metal concentrations in the floodplain sediments that are likely to be related to mining in the catchment that peaked during medieval times (ca. 1450–1780 CE; Markl, 2016). Another sign of anthropogenic catchment perturbations is the significantly elevated sedimentation rates since 0.37–0.82 ka. These increased modern rates (factor of 3.7) and, with that, overbank fine thicknesses relative to the subtle (small, short) variations in climatological conditions cannot solely be the consequence of natural factors.

#### 6 Conclusions

Our study presents insights into the geomorphological history of the shift from a naturally to anthropogenically controlled meso-scale central European fluvial catchment, with a special focus on floodplain sediment contamination by heavy metals, using sedimentological and geochemical measurements, luminescence dating, and geophysical surveys. It contributes counterweight to the extensive body of literature focusing on micro- and macro-fluvial systems. Our observations reveal that the Kinzig overbank fines are underlain by Pleistocene fluvial gravel that gradually transitions into sandy layers and, finally, into fine-grained flood loams closer to the surface. This transition is likely to be associated with climatic shifts at the Pleistocene-Holocene boundary that changed the braiding character of the Kinzig into, ultimately, a single-thread channel, enabling floodplain development storing sandy and, later, silty sediments. After several thousands of years with stable sedimentation rates between ca. 12.9 ka and 0.82 ka, the onset of anthropogenic activities in the upstream catchment areas triggered an enhanced influx of silty material. According to OSL dating, sedimentation rates increased sharply between 0.82 and 0.37 ka, leading to the deposition of thick flood loams. These fines contain elevated OM contents and enhanced heavy metal concentrations (enrichment factors of ca. 3) that are likely to be related to the mining in the catchment, which stimulated deforestation and, with that, hillslope instability, which affected sediment delivery to the fluvial system. These peaks in heavy metal concentrations coincide with the documented peaks in mining and ore processing in the catchment.

Although a clear distinction between climatic and anthropogenic forcings was not achieved, the trend in grain size and heavy metal concentrations over time implies that the fluvial system transition was induced by local anthropogenic land use impacts. A gradual shift from a mainly natural system to an anthropogenically altered system took place since human settlement, which intensified in the last ca. 1.0 ka. The an-

thropogenic external forcings on the system behind this transition are of key importance for assessing the resilience of the hydrological and sedimentological systems that were under stress already due to changing climatic conditions.

Further enhancing our understanding of the response of fluvial systems to anthropogenic drivers should include a larger focus on regional comparison and different spatial scales to unravel unique fingerprints of anthropogenic influences with regard to geologically and hydrologically defined fluvial systems. Namely, in order to understand the extent and pathways of human impact, the natural fluvial system needs to be understood first.

Future work in the Kinzig floodplains should further test the robustness of the approximate IRSL ages by increasing the sampling density in the field. In combination with OSL dating, cost-efficient IRSL age approximations could be developed into a robust dating-proxy method. In addition, attenuation of upstream to downstream catchment perturbations in floodplain sediments could be studied in the downstream Kinzig catchment as timber drift and rafting, as well as mining, were not predominant there. It is expected that downstream floodplain archives captured attenuated signals of the same anthropogenic impacts.

Code and data availability. The digital elevation data of this study were freely accessed via the Landesamt für Geoinformation und Landentwicklung (State Office for Geoinformation and Rural Development) portal (LGL, https://www.lgl-bw.de/, last access: 4 November 2025, dl-de/by-2-0). The Supplement contains additional data and information on data (pre)processing. All other data will be made available upon request to the authors.

**Supplement.** The supplement related to this article is available online at https://doi.org/10.5194/egqsj-74-235-2025-supplement.

**Author contributions.** CE: conceptualisation, methodology, investigation, analysis, visualisation, validation, writing (original draft). FP: funding acquisition, supervision, conceptualisation, methodology, analysis, validation. AF: investigation, visualisation, validation. JW: investigation, validation. EE: investigation, validation. DQ: investigation, validation. SH: analysis, visualisation, validation. JB: funding acquisition, supervision, conceptualisation, methodology, analysis, validation, writing (original draft).

**Competing interests.** The contact author has declared that none of the authors has any competing interests.

**Disclaimer.** Publisher's note: Copernicus Publications remains neutral with regard to jurisdictional claims made in the text, published maps, institutional affiliations, or any other geographical representation in this paper. While Copernicus Publications makes every effort to include appropriate place names, the final responsibil-

ity lies with the authors. Views expressed in the text are those of the authors and do not necessarily reflect the views of the publisher.

**Special issue statement.** This article is part of the special issue "Floodplain architecture of fluvial anthropospheres". It is not associated with a conference.

Acknowledgements. Our publication is part of a DFG-funded project within the Special Priority Programme 2361 "On the Way to the Fluvial Anthroposphere". We thank the landowners and municipality of Schenkenzell for the access to and insights into their land, the experts for the sharing of their knowledge and the relevant literature (Werner Konold, Hans Harter, Heiko Wagner, and Willy Schoch), and our colleagues for their assistance during the fieldwork (Mubarak Abdulkarim, Lucia Götz, Jahir Rangel, Leonie Frick, Veronica Cordero, and Martin Kügel) and laboratory analyses (Margarita Nuss, Savanna Kager, Jennifer Wolff, and Janine Wagner).

**Financial support.** This research has been supported by the Deutsche Forschungsgemeinschaft (grant no. 509914528).

This open-access publication was funded by the University of Freiburg.

**Review statement.** This paper was edited by Frank Lehmkuhl and reviewed by two anonymous referees.

#### References

- Aarhus GeoSoftware: RES2DINVx64, https://www.aarhusgeosoftware.dk/download-resxdinv (last access: 23 January 2024), 2022.
- Abdulkarim, M., Grema, H. M., Adamu, I. H., Mueller, D., Schulz, M., Ulbrich, M., Miocic, J. M., and Preusser, F.: Effect of using different chemical dispersing agents in grain size analyses of fluvial sediments via laser diffraction spectrometry, Methods and Protocols, 4, 44, https://doi.org/10.3390/mps4030044, 2021.
- Abdulkarim, M., Schmitt, L., Fülling, A., Rambeau, C., Ertlen, D., Mueller, D., Chapkanski, S., and Preusser, F.: Late glacial to Holocene fluvial dynamics in the Upper Rhine alluvial plain, France, Quaternary Res., 121, 109–131, https://doi.org/10.1017/qua.2024.22, 2024.
- Archie, G. E.: The Electrical Resistivity Log as an Aid in Determining Some Reservoir Characteristics, Transactions of the AIME, 146, 54–62, https://doi.org/10.2118/942054-G, 1941.
- Barth, L.: Die Geschichte der Flößerei im Flußgebiet der oberen Kinzig – ein Beitrag zur Geschichte der Schwarzwälder Schifferschaften, dissertation, urn:nbn:de:bvb:12-bsb11539101-5, München, Univ., https://www.deutsche-digitale-bibliothek. de/item/BPFN57JJO5PBYZ5JY5AWZY3JFUJM6PDK (last access: 21 July 2023), 1895.
- Belletti, B., de Leaniz, C. G., Jones, J., Bizzi, S., Börger, L., Segura, G., Castelletti, A., van de Bund, W., Aarestrup, K., Barry,

- J., Belka, K., Berkhuysen, A., Birnie-Gauvin, K., Bussettini, M., Carolli, M., Consuegra, S., Dopico, E., Feierfeil, T., Fernández, S., Garrido, P. F., Garcia-Vazquez, E., Garrido, S., Giannico, G., Gough, P., Jepsen, N., Jones, P. E., Kemp, P., Kerr, J., King, J., Łapińska, M., Lázaro, G., Lucas, M. C., Marcello, L., Martin, P., McGinnity, P., O'Hanley, J., del Amo, R. O., Parasiewicz, P., Pusch, M., Rincon, G., Rodriguez, C., Royte, J., Schneider, C. T., Tummers, J. S., Vallesi, S., Vowles, A., Verspoor, E., Wanningen, H., Wantzen, K. M., Wildman, L., and Zalewski, M.: More than one million barriers fragment Europe's rivers, Nature, 588, 436–441, https://doi.org/10.1038/s41586-020-3005-2, 2020.
- Blanchy, G., Saneiyan, S., Boyd, J., McLachlan, P., and Binley, A.: ResIPy, an intuitive open source software for complex geoelectrical inversion/modeling, Computers and Geosciences, 137, 104423, https://doi.org/10.1016/j.cageo.2020.104423, 2020.
- Bliedtner, M. and Martin, M.: Erz- und Minerallagerstätten des Mittleren Schwarzwaldes, dissertation, idn=880715510, https://d-nb.info/880715510 (last access: 21 August 2023), 1986.
- Blott, S. J. and Pye, K.: Gradistat: A grain size distribution and statistics package for the analysis of unconsolidated sediments, Earth Surf. Proc. Land., 26, 1237–1248, https://doi.org/10.1002/esp.261, 2001.
- Bork, H.-R.: Landschaftsentwicklung in Mitteleuropa: Wirkungen des Menschen auf Landschaften, Klett, ISBN 3-623-00849-4, 1998.
- Bösmeier, A. S., Himmelsbach, I., and Seeger, S.: Reliability of flood marks and practical relevance for flood hazard assessment in southwestern Germany, Nat. Hazards Earth Syst. Sci., 22, 2963–2979, https://doi.org/10.5194/nhess-22-2963-2022, 2022.
- Braun, G.: Beiträge zur Hydrographie des Grossherzogthums Baden Karten zum Fünften Heft: Der Binnenflussbau im Grossherzogthum Baden, URN: urn:nbn:de:bvb:12-bsb11485971-2, 1887.
- Bronk Ramsey, C.: Bayesian analysis of radiocarbon dates, Radiocarbon, 51, 337–360, https://doi.org/10.1017/s0033822200033865, 2009.
- Broothaerts, N., Notebaert, B., Verstraeten, G., Kasse, C., Bohncke, S., and Vandenberghe, J.: Non-uniform and diachronous Holocene floodplain evolution: A case study from the Dijle catchment, Belgium, J. Quaternary Sci., 29, 351–360, https://doi.org/10.1002/jqs.2709, 2014.
- Brown, A. G., Toms, P., Carey, C., and Rhodes, E.: Geomorphology of the Anthropocene: Time-transgressive discontinuities of human-induced alluviation, Anthropocene, 1, 3–13, https://doi.org/10.1016/j.ancene.2013.06.002, 2013.
- Brown, A. G., Lespez, L., Sear, D. A., Macaire, J. J., Houben, P., Klimek, K., Brazier, R. E., Oost, K. V., and Pears, B.: Natural vs anthropogenic streams in Europe: History, ecology and implications for restoration, river-rewilding and riverine ecosystem services, Earth-Sci. Rev., 180, 185–205, https://doi.org/10.1016/j.earscirev.2018.02.001, 2018.
- Bund/Länder-Arbeitsgemenschaft Bodemschutz (LABO): Hintergrundwerte für anorganische und organische Stoffe in Böden Anhang: Tabellen der Hintergrundwerte für Böden, https://www.labo-deutschland.de/documents/LABO\_HGW\_Anhang\_02\_2017.pdf (last access: 30 September 2024), 2017.
- Dambeck, R. and Thiemeyer, H.: Fluvial history of the northern Upper Rhine River (southwestern Germany) during the

- Lateglacial and Holocene times, Quatern. Int., 93–94, 53–63, https://doi.org/10.1016/S1040-6182(02)00006-X, 2002.
- De Moor, J. J. W., Kasse, C., Van Balen, R., Vandenberghe, J., and Wallinga, J.: Human and climate impact on catchment development during the Holocene Geul River, the Netherlands, Geomorphology, 98, 316–339, https://doi.org/10.1016/j.geomorph.2006.12.033, 2008.
- Dix, A., Burggraaff, P., Kleefeld, K.-D., Küster, H., Schirmer, W., and Zimmermann, A.: Human impact and vegetation change, Erdkunde, 59, https://doi.org/10.3112/erdkunde.2005.03.06, 2005.
- Dotterweich, M.: The history of soil erosion and fluvial deposits in small catchments of central Europe: Deciphering the long-term interaction between humans and the environment A review, Geomorphology, 101, 192–208, https://doi.org/10.1016/j.geomorph.2008.05.023, 2008.
- Elznicová, J., Kiss, T., von Suchodoletz, H., Bartyik, T., Sipos, G., Lend'áková, Z., Fačevicová, K., Pavlů, I., Kovárník, J., and Matys Grygar, T.: Was the termination of the Jizera River meandering during the Late Holocene caused by anthropogenic or climatic forcing?, Earth Surf. Proc. Land., 48, 669–686, https://doi.org/10.1002/esp.5509, 2023.
- Erkens, G., Dambeck, R., Volleberg, K. P., Bouman, M. T., Bos, J. A., Cohen, K. M., Wallinga, J., and Hoek, W. Z.: Fluvial terrace formation in the northern Upper Rhine Graben during the last 20 000 years as a result of allogenic controls and autogenic evolution, Geomorphology, 103, 476–495, https://doi.org/10.1016/j.geomorph.2008.07.021, 2009.
- Euzen, C., Chabaux, F., Rixhon, G., Preusser, F., Eyrolle, F., Chardon, V., Zander, A. M., Badariotti, D., and Schmitt, L.: Multi-method geochronological approach to reconstruct post-1800 floodplain sedimentation in the upper Rhine plain, France, Quat. Geochronol., 83, https://doi.org/10.1016/j.quageo.2024.101561, 2024.
- Foellmer, A.: Schwermetalleinträge durch den Schwarzwälder Bergbau in die südliche Oberrheinebene zwischen Möhlin und Sulzbach, in: Freiburger Geowissenschaftliche Beiträge, Freiburg Geologisches Institut der Albert-Ludwigs-Universität Freiburg, ISSN 0936-6571, 1999.
- Friedmann, A.: Die spät- und postglaziale Landschafts- und Vegetationsgeschichte des südlichen Oberrheintieflands und Schwarzwalds, Freiburger geographische Hefte, H. 62, https://portal.dnb.de/opac.htm?method=simpleSearch&cqlMode=true&query=idn=967481791 (last access: 16 September 2024), 2000.
- Friedmann, A.: Holocene vegetation, land use and settlement in the Black Forest, Berichte Geographie und Landeskunde, 76, 187–205, https://www.researchgate.net/publication/289274094 (last access: 13 September 2024), 2002.
- Fryirs, K.: (Dis)Connectivity in catchment sediment cascades: a fresh look at the sediment delivery problem. Earth Surf. Proc. Land., 38, 30–46, https://doi.org/10.1002/esp.3242, 2013.
- Fuchs, M., Fischer, M., and Reverman, R.: Colluvial and alluvial sediment archives temporally resolved by OSL dating: Implications for reconstructing soil erosion, Quat. Geochronol., 5, 269– 273, https://doi.org/10.1016/j.quageo.2009.01.006, 2010.
- Fuchs, M., Will, M., Kunert, E., Kreutzer, S., Fischer, M., and Reverman, R.: The temporal and spatial quantification of Holocene sediment dynamics in a meso-scale catchment

- in northern Bavaria, Germany, The Holocene, 21, 1093–1104, https://doi.org/10.1177/0959683611400459, 2011.
- Fuchs, M. C., Kreutzer, S., Burow, C., Dietze, M., Fischer, M., Schmidt, C., and Fuchs, M.: Data processing in luminescence dating analysis: An exemplary workflow using the R package 'Luminescence', Quatern. Int., 362, 8–13, https://doi.org/10.1016/j.quaint.2014.06.034, 2015.
- Galbraith, R. F., Roberts, R. G., Laslett, G. M., Yoshida, H., and Olley, J. M.: Optical dating of single and multiple grains of quartz from Jinmium rock shelter, northern Australia: Part I, experimental design and statistical models, Archaeometry, 41, 339–364, https://doi.org/10.1111/j.1475-4754.1999.tb00987.x, 1999.
- Galia, T.: Legacy of human impact on geomorphic processes in mountain headwater streams in the perspective of european cultural land scapes, Geosciences (Switzerland), 11, 253, https://doi.org/10.3390/geosciences11060253, 2021.
- Gegg, L. and Gegg, J.: Poor Man's Line Scan a simple tool for the acquisition of high-resolution, undistorted drill core photos, Sci. Dril., 32, 55–59, https://doi.org/10.5194/sd-32-55-2023, 2023.
- Gibling, M. R.: River Systems and the Anthropocene: A Late Pleistocene and Holocene Timeline for Human Influence, Quaternary, 1, 21, https://doi.org/10.3390/quat1030021, 2018.
- Glaser, R. and Riemann, D.: A thousand-year record of temperature variations for Germany and central Europe based on documentary data, J. Quaternary Sci., 24, 437–449, https://doi.org/10.1002/jqs.1302, 2009.
- Grygar, T. M., Nováková, T., Bábek, O., Elznicová, J., and Vadinová, N.: Robust assessment of moderate heavy metal contamination levels in floodplain sediments: A case study on the Jizera River, Czech Republic, Sci. Total Environ., 452–453, 233–245, https://doi.org/10.1016/j.scitotenv.2013.02.085, 2013.
- Harter, H.: Schiltacher Schiffer an Wutach, Hochrhein, Bodensee und Kinzig, Die Ortenau: Zeitschrift des Historischen Vereins für Mittelbaden, 91, 31–60, 2011.
- Heidelberg, U.: Topographische Karte über das Grossherzogthum Baden: nach der allgemeinen Landesvermessung des Großherzoglichen militairisch topographischen Bureaus: Eberbach 1838–1849, https://doi.org/10.11588/diglit.24019#0002, 1849.
- Heiri, O., Lotter, A. F., and Lemcke, G.: Loss on ignition as a method for estimating organic and carbonate content in sediments: Reproducibility and comparability of results, J. Paleolimnol., 25, 101–110, https://doi.org/10.1023/A:1008119611481, 2001.
- Himmelsbach, I.: Erfahrung-Mentalität-Management Hochwasser und Hochwasserschutz an den nicht-schiffbaren Flüssen im Ober-Elsass und am Oberrhein (1480–2007), URN: urn:nbn:de:bsz:25-opus-89694, 2012.
- Hoevers, R., Broothaerts, N., and Verstraeten, G.: Holocene geoecohydrological floodplain dynamics in NE Belgium: regional drivers of local change, J. Quaternary Sci., 39, 781–800, https://doi.org/10.1002/jqs.3621, 2024.
- Hoffmann, T., Erkens, G., Cohen, K. M., Houben, P., Seidel, J., and Dikau, R.: Holocene floodplain sediment storage and hill-slope erosion within the Rhine catchment, Holocene, 17, 105–118, https://doi.org/10.1177/0959683607073287, 2007a.
- Hoffmann, T., Lang, A., and Dikau, R.: The challenge of reconstructing human impact on large river systems, PAGES news, 15, 21–23, https://doi.org/10.22498/pages.15.1.21, 2007b.

- Hoffmann, T., Lang, A., and Dikau, R.: Holocene river activity: analysing 14C-dated fluvial and colluvial sediments from Germany, Quaternary Sci. Rev., 27, 2031–2040, https://doi.org/10.1016/j.quascirev.2008.06.014, 2008.
- Hoffmann, T., Erkens, G., Gerlach, R., Klostermann, J., and Lang, A.: Trends and controls of Holocene floodplain sedimentation in the Rhine catchment, Catena, 77, 96–106, https://doi.org/10.1016/j.catena.2008.09.002, 2009.
- Hohensinner, S., Grupe, S., Klasz, G., and Payer, T.: Long-term deposition of fine sediments in Vienna's Danube floodplain before and after channelization, Geomorphology, 398, 108038, https://doi.org/10.1016/j.geomorph.2021.108038, 2022.
- Holzhauer, I., Kadereit, A., Schukraft, G., Kromer, B., and Bubenzer, O.: Spatially heterogeneous relief changes, soil formation and floodplain aggradation under human impact geomorphological results from the Upper Rhine Graben (SW Germany), Zeitschrift fur Geomorphologie, 61, 121–158, https://doi.org/10.1127/zfg\_suppl/2017/0357, 2017.
- Houben, P.: Sediment budget for five millennia of tillage in the Rockenberg catchment (Wetterau loess basin, Germany), Quaternary Sci. Rev., 52, 12–23, https://doi.org/10.1016/j.quascirev.2012.07.011, 2012.
- Houben, P., Hoffmann, T., Zimmermann, A., and Dikau, R.: Land use and climatic impacts on the Rhine system (RheinLUCIFS): Quantifying sediment fluxes and human impact with available data, Catena, 66, 42–52, https://doi.org/10.1016/j.catena.2005.07.009, 2006.
- IRIS Instruments: Prosys III, v. 2.11, https://www.iris-instruments.com/download.html# (last access: 30 January 2024), 2024.
- Jain, M., Murray, A. S., and Botter-Jensen, L.: Optically stimulated luminescence dating: how significant is incomplete light exposure in fluvial environments? [Datation par luminescence stimulée optiquement : quelle signification en cas de blanchiment incomplet des sédiments fluviatiles?], Quaternaire, 15, 143–157, https://doi.org/10.3406/quate.2004.1762, 2004.
- James, L. A.: Legacy sediment: Definitions and processes of episodically produced anthropogenic sediment, Anthropocene, 2, 16–26, https://doi.org/10.1016/j.ancene.2013.04.001, 2013.
- Kalis, A. J., Merkt, J., and Wunderlich, J.: Environmental changes during the Holocene climatic optimum in central Europe - human impact and natural causes, Quaternary Sci. Rev., 22, 33–79, https://doi.org/10.1016/S0277-3791(02)00181-6, 2003.
- Kanianska, R., Varga, J., Benková, N., Kizeková, M., and Jančová, L.: Floodplain soils contamination assessment using the sequential extraction method of heavy metals from past mining activities, Scientific Reports, 12, https://doi.org/10.1038/s41598-022-06929-7, 2022.
- Knausenberger, G.: Der Kinzigtäler Bergbau eine Zusammenfassung über Gesichertes und Ungesichertes, Die Ortenau, ISSN 2698-4385, 2001.
- Konold, W., Suchomel, C., and Hugelmann, M.: Riesen, Schwallungen, Flößerei - Eine Studie zur Kultur- und Baugeschichte der Holzbringungsanlagen im Einzugsgebiet der oberen Kinzig, Allemanisches Jahrbuch 2019/2020, https://doi.org/10.57962/regionalia-22661, 2019.
- Lang, A.: Phases of soil erosion-derived colluviation in the loess hills of South Germany, Catena, 51, 209–221, https://doi.org/10.1016/S0341-8162(02)00166-2, 2003.

- Lang, A. and Honscheidt, S.: Age and source of colluvial sediments at Vaihingen-Enz, Germany, Catena, 38, 89–107, 1999.
- Lang, A., Bork, H. R., Mäckel, R., Preston, N., Wunderlich, J., and Dikau, R.: Changes in sediment flux and storage within a fluvial system: Some examples from the Rhine catchment, Hydrol. Process., 17, 3321–3334, https://doi.org/10.1002/hyp.1389, 2003.
- Larsen, A., Bork, H. R., Fuelling, A., Fuchs, M., and Larsen, J. R.: The processes and timing of sediment delivery from headwaters to the trunk stream of a Central European mountain gully catchment, Geomorphology, 201, 215–226, https://doi.org/10.1016/j.geomorph.2013.06.022, 2013.
- Lehmann, B.: Die Kinzig und die Flösserei, Flößerei- und Verkehrsmuseum Gengenbach, Huber Druck und Verlag, Offenburg, 2005.
- LGRB: Landesamt für Geologie, Rohstoffe und Bergbau: Fachanwendungen und Fachthemen Geologie Geologische Übersichtskarte 1:300000 (GÜK300) GÜK300: Geologische Einheiten, https://maps.lgrb-bw.de/ (last access: 8 February 2024), 2024.
- Loke, M. H.: Tutorial: 2-D and 3-D electrical imaging surveys, http://www.geoelectrical.com (last access: 6 December 2024), 2004.
- Longoni, R.: Floodplains through the letter Land use and fluvial dynamics in the Upper Rhine area reconstructed from written sources, 1200-1700, in: Mittelalter, Interdisziplinäre Forschung und Rezeptionsgeschichte, 7, 41–45, https://doi.org/10.26012/mittelalter-34427, 2024.
- LUBW: Landesanstalt für Umwelt Baden-Württemberg: Bodenzustandsbericht Ortenaukreis, https://pudi.lubw.de/detailseite/-/publication/85762/ (last access: 3 July 2025), 2014.
- LUBW: Landesanstalt für Umwelt Baden-Württemberg: Hochwasservorhersagezentrale HVZ-Pegelkarte, https://hvz.lubw.badenwuerttemberg.de/ (last access: 24 April 2024), 2024.
- Ludemann, T.: Past fuel wood exploitation and natural forest vegetation in the Black Forest, the Vosges and neighbouring regions in western Central Europe, Palaeogeogr. Palaeocl., 291, 154–165, https://doi.org/10.1016/j.palaeo.2009.09.013, 2010.
- Maaß, A. L., Schüttrumpf, H., and Lehmkuhl, F.: Human impact on fluvial systems in Europe with special regard to today's river restorations, Environmental Sciences Europe, 33, 119, https://doi.org/10.1186/s12302-021-00561-4, 2021.
- Mäckel, R.: Naturraum und Relief, Ber. Naturf. Ges. Freiburg i. Br, 90, 9–28, https://www.zobodat.at/ (last access: 13 September 2024), 2000.
- Mäckel, R. and Friedmann, A.: Holozäner Landschaftswandel im südlichen Oberrheintiefland und Schwarzwald, E&G Quaternary Sci. J., 49, 1–20, https://doi.org/10.3285/eg.49.1.01, 1999.
- Mäckel, R. and Metz, B.: Spät- und postglaziale Fluss Aktivität im Schwarzwald und Oberrheintiefland, in: Schwarzwald und Oberrheintiefland: eine Einführung in das Exkursionsgebiet um Freiburg im Breisgau, Freiburger geographische Hefte, H. 36, 82–103, 1992.
- Mäckel, R. and Thomas, U.: Die Oberflächenformung des Zartener Beckens im Spät-und Postglazial, Ber. Naturf. Ges. Freiburg i. Br, 99, 45–76, https://www.zobodat.at/ (last access: 3 October 2024), 2009.
- Mäckel, R., Ries, J. B., and Friedmann, A. M.: Der Einfluß des Menschen auf die Auensedimentation im Schwarzwald und Oberrheintiefland, Berichte der naturforschenden Gesellschaft

- zu Freiburg im Breisgau, 86–87, 43–54, https://www.zobodat. at/pdf/Berichte-naturf-Ges-Freiburg-Br\_86-87\_0043-0054.pdf (last access: 3 October 2024), 1996.
- Mäckel, R., Schneider, R., Friedmann, A., and Seidel, J.: Environmental Changes and Human Impact on the Relief Development in the Upper Rhine Valley and Black Forest (South-West Germany) during the Holocene, Zeitschrift für Geomorphologie, 128, 31–45, https://www.researchgate.net/publication/284183362 (last access: 13 September 2024), 2002.
- Mäckel, R., Schneider, R., and Seidel, J.: Anthropogenic impact on the landscape of southern Badenia (Germany) during the Holocene – Documented by colluvial and alluvial sediments, Archaeometry, 45, 487–501, https://doi.org/10.1111/1475-4754.00123, 2003.
- Mäckel, R., Friedmann, A., and Sudhaus, D.: Environmental changes and human impact on landscape development in the upper rhine region, Erdkunde, 63, 35–49, https://doi.org/10.3112/erdkunde.2009.01.03, 2009.
- Macklin, M. G., Passmore, D. G., and Rumsby, B. T.: The use of overbank sediment for geochemical mapping and contamination assessment: results from selected English and Welsh floodplains, Appl. Geochem., 9, 689–700, https://doi.org/10.1016/0883-2927(94)90028-0, 1994.
- Macklin, M. G., Jones, A. F., and Lewin, J.: River response to rapid Holocene environmental change: evidence and explanation in British catchments, Quaternary Sci. Rev., 29, 1555–1576, https://doi.org/10.1016/j.quascirev.2009.06.010, 2010.
- Macklin, M. G., Thomas, C. J., Mudbhatkal, A., Brewer, P. A., Hudson-Edwards, K. A., Lewin, J., Scussolini, P., Eilander, D., Lechner, A., Owen, J., Bird, G., Kemp, D., and Mangalaa, K. R.: Impacts of metal mining on river systems: a global assessment, Science, 381, 1345–1350, https://doi.org/10.1126/science.adg6704, 2023.
- Markl, G.: Mittlerer Schwarzwald Lagerstätten und Mineralien aus vier Jahrhunderten, Bode, D., ISBN 978-3-942588-24-9, 2016.
- Mathewes, R. W.: Plant macrofossils as indicators of vegetation and climate change in the Northern Black Forest of Germany during the last millennium with focus on the Little Ice Age, Vegetation History and Archaeobotany, 32, 111–123, https://doi.org/10.1007/s00334-022-00885-y, 2023.
- May, J. H., Preusser, F., and Gliganic, L. A.: Refining late Quaternary plunge pool chronologies in Australia's monsoonal 'Top End', Quat. Geochronol., 30, 328–333, https://doi.org/10.1016/j.quageo.2015.01.008, 2015.
- Merz, W.: Böden, fluviale Morphodynamik und Talgeschichte in den Quelltälern der Schiltach, Mittlerer Schwarzwald, unpublished state exam, 1987.
- Murray, A. S. and Wintle, A. G.: The single aliquot regenerative dose protocol: Potential for improvements in reliability, Radiation Measurements, 37, 377–381, https://doi.org/10.1016/S1350-4487(03)00053-2, 2003.
- Notebaert, B. and Verstraeten, G.: Sensitivity of West and Central European river systems to environmental changes during the Holocene: A review, Earth-Sci. Rev., 103, 163–182, https://doi.org/10.1016/j.earscirev.2010.09.009, 2010.
- Notebaert, B., Verstraeten, G., Ward, P., Renssen, H., and Van Rompaey, A.: Modeling the sensitivity of sediment and water runoff dynamics to Holocene climate and land use

- changes at the catchment scale, Geomorphology, 126, 18–31, https://doi.org/10.1016/j.geomorph.2010.08.016, 2011.
- Notebaert, B., Broothaerts, N., and Verstraeten, G.: Evidence of anthropogenic tipping points in fluvial dynamics in Europe, Global Planet. Change, 164, 27–38, https://doi.org/10.1016/j.gloplacha.2018.02.008, 2018.
- Pennock, D., Lefevre, C., and Vargas, R.: Soil erosion: the greatest challenge for sustainable soil management, FAO, 1st edn., ISBN 978-92-5-131426-5, 2019.
- Preusser, F.: Characterisation evolution of and the River Rhine system, Geologie en Miinbouw/Netherlands Journal of Geosciences, 87, 7-19,https://doi.org/10.1017/S0016774600024008, 2008.
- Quandt, D., Busch, B., Greve, J., and Hilgers, C.: Rock characteristics and reservoir properties of Upper Carboniferous (Stephanian A–B) tight siliciclastic rocks from the Saar–Nahe basin (SW Germany), International Journal of Earth Sciences, 113, https://doi.org/10.1007/s00531-024-02394-x, 2024.
- Reimann, C. and de Caritat, P.: Distinguishing between natural and anthropogenic sources for elements in the environment: Regional geochemical surveys versus enrichment factors, Sci. Total Environ., 337, 91–107, https://doi.org/10.1016/j.scitotenv.2004.06.011, 2005.
- Reimer, P. J., Austin, W. E., Bard, E., Bayliss, A., Blackwell, P. G., Bronk Ramsey, C. B., Butzin, M., Cheng, H., Edwards, R. L., Friedrich, M., Grootes, P. M., Guilderson, T. P., Hajdas, I., Heaton, T. J., Hogg, A. G., Hughen, K. A., Kromer, B., Manning, S. W., Muscheler, R., Palmer, J. G., Pearson, C., Plicht, J. V. D., Reimer, R.W., Richards, D. A., Scott, E. M., Southon, J. R., Turney, C. S., Wacker, L., Adolphi, F., Büntgen, U., Capano, M., Fahrni, S. M., Fogtmann-Schulz, A., Friedrich, R., Köhler, P., Kudsk, S., Miyake, F., Olsen, J., Reinig, F., Sakamoto, M., Sookdeo, A., and Talamo, S.: The IntCal20 Northern Hemisphere Radiocarbon Age Calibration Curve (0–55 cal kBP), Radiocarbon, 62, 725–757, https://doi.org/10.1017/RDC.2020.41, 2020.
- Riezler, S.: Fürstenbergisches Urkundenbuch, 1. Quellen zur Geschichte der Grafen von Achalm, Urach und Fürstenberg bis zum Jahre 1299, Hauptarchiv in Donaueschingen, URN: urn:nbn:de:bvb:12-bsb11351515-5, https://www.digitale-sammlungen.de/de/details/bsb11351515 (last access: 10 September 2024), 1877.
- Rommens, T., Verstraeten, G., Bogman, P., Peeters, I., Poesen, J., Govers, G., Rompaey, A. V., and Lang, A.: Holocene alluvial sediment storage in a small river catchment in the loess area of central Belgium, Geomorphology, 77, 187–201, https://doi.org/10.1016/j.geomorph.2006.01.028, 2006.
- Rösch, M.: Pollenprofil Breitnau-Neuhof: Zum zeitlichen Verlauf der holozänen Vegetationsentwicklung im südlichen Schwarzwald, Carolinea Beiträge zur naturkundlichen Forschung in Südwestdeutschland, Carolinea, 47, 15–24, 1989.
- Rösch, M.: Abies alba and Homo sapiens in the Schwarzwald a Difficult Story, Interdisciplinaria Archaeologica, 6, https://doi.org/10.24916/iansa.2015.1.4, 2015.
- Rosgen, D. L.: A classification of natural rivers, CATENA, 22, 169–199, https://doi.org/10.1016/0341-8162(94)90001-9, 1994.
- Schauenburg, G. v.: Der Holzhandel des badischen Schwarzwaldes zwischen Waldbesitzer und erstem Abnehmer, Springer, Berlin, 1899.

- Scheifele, M.: Als die Wälder auf Reisen gingen: Wald Holz Flösserei in der Wirtschaftsgeschichte des Enz-Nagold-Gebiets, Der Kleine Buch Verlag, ISBN-10: 3765081647, 1995a.
- Scheifele, M.: Die Murgschifferschaft Geschichte des Floßhandels, des Waldes und der Holzindustrie im Murgtal, Katz, ISBN 3925825207, 1995b.
- Schulze, T., Schwahn, L., Fülling, A., Zeeden, C., Preusser, F., and Sprafke, T.: Investigating the loess–palaeosol sequence of Bahlingen-Schönenberg (Kaiserstuhl), southwestern Germany, using a multi-methodological approach, E&G Quaternary Sci. J., 71, 145–162, https://doi.org/10.5194/egqsj-71-145-2022, 2022.
- Schwahn, L., Schulze, T., Fülling, A., Zeeden, C., Preusser, F., and Sprafke, T.: Multi-method study of the Middle Pleistocene loess–palaeosol sequence of Köndringen, SW Germany, E&G Quaternary Sci. J., 72, 1–21, https://doi.org/10.5194/egqsj-72-1-2023, 2023.
- Seidel, J.: Massenbilanzen holozäner Sedimente am südlichen und mittleren Oberrhein, PhD thesis, Department of Geography, Albert-Ludwigs-Universität Freiburg, 2004.
- Sensors and Software Inc.: EKKO-Project, https://www.sensoft.ca/products/ekko-project/overview/ (last access: 2 May 2024), 2017.
- Sloot, H. A. V. D. and Kosson, D. S.: Leaching assessment methodologies for disposal and use of bauxite residues, https://www.scribd.com/document/501077498/leachingassessment-methodologies-for-disposal-and-use-of-bauxiteresidue (last access: 27 October 2025), 2010.
- Stalf, A.: Korrektion und Unterhaltung der Kinzig, Die Ortenau, URN: urn:nbn:de:bsz:25-digilib-69148, http://dl.ub.uni-freiburg.de/digilit/ortenau1932 (last access: 15 August 2023), 1932.
- Starkel, L., Soja, R., and Michczyńska, D. J.: Past hydrological events reflected in Holocene history of Polish rivers, CATENA, 66, 24–33, https://doi.org/10.1016/j.catena.2005.07.008, 2006.
- Steinle, A. and Herbener, M.: Die Floßbarmachung der Kinzig am Beispiel historischer Schwallungen: Auswirkungen auf die Gewässerökologie in Vergangenheit und Gegenwart sowie zukünftige Erhaltungs-und Nutzungspotentiale, https://www.zobodat.at/publikation\_articles.php?id=310392 (last access: 21 June 2023), 2016.
- Stolz, C., Grunert, J., and Fülling, A.: Quantification and dating of floodplain sedimentation in a medium-sized catchment of the German uplands: A case study from the Aar Valley in the southern Rhenish Massif, Germany, Die Erde, 144, 30–50, https://doi.org/10.12854/erde-144-3, 2013.
- Straßburger, M.: Mining archaeology of Schnellingen at Haslach in the Kinzig valley, Central Black Forest, in: Vergessenes Wissen - historische Methoden und Technologien in der europäischen Montangeschichte, edited by: Silvertant, J., 12th Yearbook of the Institute Europa Subterranea 2016, Freiberg/Gulpen 2017, 6–45, 2017.
- Sudhaus, D. and Friedmann, A.: Late-Glacial and Holocene Geomorphodynamics and Landscape Development in the Eastern Black Forest, Zeitschrift für Geomorphologie Supplementary Issues, 142, 195–205, https://www.researchgate.net/publication/284183528 (last access: 13 September 2024), 2006.

- Sun, H., Nelson, M., Chen, F., and Husch, J.: Soil mineral structural water loss during loss on ignition analyses, Canadian Journal of Soil Science, 89, 603–610, https://doi.org/10.4141/CJSS09007, 2009
- Szabó, Z., Buró, B., Szabó, J., Tóth, C. A., Baranyai, E., Herman, P., Prokisch, J., Tomor, T., and Szabó, S.: Geomorphology as a driver of heavy metal accumulation patterns in a floodplain, Water (Switzerland), 12, 563, https://doi.org/10.3390/w12020563, 2020
- Tockner, K., Tonolla, D., Bremerich, V., Jähnig, S. C., Robinson, C. T., and Zarfl, C.: Introduction to European rivers, Elsevier, 1–26, https://doi.org/10.1016/B978-0-08-102612-0.00001-8, ISBN 9780081026120, 2022.
- Trimble, S.: Decreased rates of alluvial sediment storage in the Coon Creek Basin, Wisconsin, 1975–93, Science, 285, 1244–1246, https://doi.org/10.1126/science.285.5431.1244, 1999.
- Verstraeten, G., Broothaerts, N., Loo, M. V., Notebaert, B., D'Haen, K., Dusar, B., and Brue, H. D.: Variability in fluvial geomorphic response to anthropogenic disturbance, Geomorphology, 294, 20–39, https://doi.org/10.1016/j.geomorph.2017.03.027, 2017.
- von Suchodoletz, H., Khosravichenar, A., Fütterer, P., Zielhofer, C., Schneider, B., Sprafke, T., Tinapp, C., Fülling, A., Werther, L., Stäuble, H., Hein, M., Veit, U., Ettel, P., Werban, U., and Miera, J.: Holocene overbank sedimentation in Central Europe between natural and human drivers The Weiße Elster River (Central Germany), Geomorphology, 449, https://doi.org/10.1016/j.geomorph.2024.109067, 2024.
- Wallinga, J.: Optically stimulated luminescence dating of fluvial deposits: a review, Boreas, 31, 303–322, https://doi.org/10.1111/j.1502-3885.2002.tb01076.x, 2002.
- Walter, R. C. and Merritts, D. J.: Natural Streams and the Legacy of Water-Powered Mills, Science, 319, 299–304, https://doi.org/10.1126/science.1151716, 2008.
- Weber, A. and Lehmkuhl, F.: Mixed response of trace element concentrations in fluvial sediments to a flash flood in a former mining area, Environmental Sciences Europe, 36, https://doi.org/10.1186/s12302-024-00926-5, 2024.
- Werner, W. and Dennert, V.: Lagerstätten und Bergbau im Schwarzwald Ein Führer unter besonderer Berücksichtigung der für die Öffentlichkeit zugänglichen Bergwerke, Landesamt für Geologie, Rohstoffe und Bergbau Baden-Württemberg, ISBN-10: 3000146369, 2004.
- Werther, L., Mehler, N., Schenk, G. J., and Zielhofer, C.: On the way to the fluvial anthroposphere – current limitations and perspectives of multidisciplinary research, Water, 13, 2188, https://doi.org/10.3390/w13162188, 2021.
- Wohl, E.: Legacy effects on sediments in river corridors, Earth-Sci. Rev., 147, 30–53, https://doi.org/10.1016/j.earscirev.2015.05.001, 2015.
- Ziegler, P.: Cenozoic rift system of Western and Central Europe: an overview, Geologie en Mijnbouw, 73, 99–127, 1994.
- Zolitschka, B., Behre, K.-E., and Schneider, J. U.: Human and climatic impact on the environment as derived from colluvial, fluvial and lacustrine archives examples from the Bronze Age to the Migration period, Germany, Quaternary Sci. Rev., 22, 81–100, 2003.